

---

# Fast Rank-1 Lattice Targeted Sampling for Black-box Optimization

---

Anonymous Author(s)

Affiliation

Address

email

## Abstract

1 Black-box optimization has gained great attention for its success in recent ap-  
2 plications. However, scaling up to high-dimensional problems with good query  
3 efficiency remains challenging. This paper proposes a novel Rank-1 Lattice Tar-  
4 geted Sampling (RLTS) technique to address this issue. Our RLTS benefits from  
5 random rank-1 lattice Quasi-Monte Carlo, which enables us to perform fast local  
6 exact Gaussian processes (GP) training and inference with  $O(n \log n)$  complexity  
7 w.r.t.  $n$  batch samples. Furthermore, we developed a fast coordinate searching  
8 method with  $O(n \log n)$  time complexity for fast targeted sampling. The fast  
9 computation enables us to plug our RLTS into the sampling phase of stochastic op-  
10 timization methods. This improves the query efficiency while scaling up to higher  
11 dimensional problems than Bayesian optimization. Moreover, to construct rank-1  
12 lattices efficiently, we proposed a closed-form construction. Extensive experiments  
13 on challenging benchmark test functions and black-box prompt fine-tuning for  
14 large language models demonstrate the query efficiency of our RLTS technique.

## 15 1 Introduction

16 Black-box optimization has gained great attention for its success in many recent applications, such as  
17 prompt fine-tuning for large language models Sun et al. [2022b,a], policy search for robot control  
18 and reinforcement learning Choromanski et al. [2019], Lizotte et al. [2007], Barsce et al. [2017],  
19 Salimans et al. [2017], automatic hyper-parameters tuning in machine learning problems Snoek  
20 et al. [2012], black-box architecture search in engineering design Wang and Shan [2007], drug  
21 discovery Negoescu et al. [2011] and accelerated simulation for scientific discovery Maddox et al.  
22 [2021], Hernández-Lobato et al. [2017], etc. Many efforts have been made for black-box optimization  
23 in the literature, including Bayesian optimization (BO) methods Srinivas et al. [2010], Gardner et al.  
24 [2017], Nayebi et al. [2019], stochastic optimization methods like evolution strategies (ES) Back et al.  
25 [1991], Hansen [2006], Wierstra et al. [2014b], Lyu and Tsang [2021] and genetic algorithms Srinivas  
26 and Patnaik [1994], Mirjalili and Mirjalili [2019].

27 Bayesian optimization usually builds a global (GP) model as a surrogate and provides queries by  
28 optimizing some acquisition functions Snoek et al. [2012]. Although BO achieves good query  
29 efficiency for low-dimensional problems, it often fails to handle high-dimensional problems with  
30 large sample budgets Eriksson et al. [2019]. The computation of GP with a large number of samples  
31 itself is expensive, and the internal optimization of the acquisition functions is challenging. Recently,  
32 Müller et al. [2021], Nguyen et al. [2022] builds a GP model for both the function value and the  
33 gradient and performs local Bayesian optimization. Although these methods improve the scalability  
34 of global BO, they usually cannot scale up to five hundred dimensional complex problems. This may  
35 be because the learned gradient heavily depends on the accuracy of the GP model. However, achieving

36 an accurate GP model is challenging for high-dimensional problems. A slightly misspecified GP  
 37 model may lead to a wrong estimated gradient due to the highly nonlinear acquisition functions.

38 On the other line, stochastic optimization methods, e.g., ES Rechenberg and Eigen [1973], Nesterov  
 39 and Spokoiny [2017], natural evolution strategies (NES) Wierstra et al. [2014b], CMAES Hansen  
 40 [2006], and implicit natural gradient optimizer (INGO) Lyu and Tsang [2021], typically sampling from  
 41 Gaussian distribution and approximate the (natural) gradient for the update of the Gaussian distribution  
 42 parameters for continuous optimization. These methods can scale up to higher dimensional problems  
 43 compared with BO. However, the gradient approximation may have a large variance, especially for  
 44 high-dimensional problems. Thus, the update direction may not be toward the descent direction,  
 45 leading to inferior query efficiency.

46 To address high-dimensional black-box problems with good query efficiency, we propose a novel  
 47 Rank-1 Lattice Targeted Sampling (RLTS) technique. Our RLTS has a  $O(n \log n)$  time complexity,  
 48 which is fast for plugging into the sampling phase of stochastic optimization methods. In this way,  
 49 our methods can improve the query efficiency of stochastic optimization methods while addressing  
 50 higher-dimensional problems than BO. Our contributions are summarized as follows:

- 51 • We propose a novel Rank-1 Lattice Targeted Sampling (RLTS) technique. Our RLTS builds  
 52 a local GP with a random rank-1 lattice, which enables fast exact GP training and inference  
 53 with  $O(n \log n)$  time complexity w.r.t.  $n$  batch samples. Furthermore, we develop a fast  
 54 coordinate search that enables target sampling with  $O(n \log n)$  time complexity.
- 55 • We propose a closed-form subgroup rank-1 lattice by considering the dual lattice regarding  
 56 the integral approximation error of functions in Korobov space. Our rank-1 lattice has a  
 57 more regular pattern of approximation error. With our closed-form subgroup rank-1 lattice,  
 58 we can perform the target sampling efficiently. Moreover, our closed-form subgroup rank-1  
 59 lattice may be potential for other applications beyond black-box optimization.
- 60 • We plug our RLTS into the sampling phase at each step of stochastic optimization methods to  
 61 improve query efficiency. In this way, during the optimization procedure, our RLTS sampling  
 62 from an updated promising region instead of a fixed one at each step. This approach can  
 63 scale up to address higher dimensional problems than most Bayesian optimization.
- 64 • Empirically, extensive experiments on high-dimensional challenging benchmark test func-  
 65 tions and practical black-box prompt fine-tuning for large language models demonstrate the  
 66 effectiveness of our RLTS technique.

## 67 2 Background

### 68 2.1 Black-box Optimization

69 Given a proper function  $f(\mathbf{x}) : \mathbb{R}^d \rightarrow \mathbb{R}$  such that  $f(\mathbf{x}) > -\infty$ , black-box optimization is to  
 70 minimize  $f(\mathbf{x})$  by using function queries only. Black-box stochastic optimization methods typically  
 71 employ a sampling distribution  $p(\mathbf{x}; \boldsymbol{\theta})$  and optimizes the parameter of the distribution regarding the  
 72 relaxed problem:  $J(\boldsymbol{\theta}) := \mathbb{E}_{p(\mathbf{x}; \boldsymbol{\theta})}[f(\mathbf{x})]$ .

73 Evolution Strategies (ES) Rechenberg and Eigen [1973], Nesterov and Spokoiny [2017] employ a  
 74 Gaussian distribution  $\mathcal{N}(\boldsymbol{\mu}, \sigma^2 \mathbf{I})$  for sampling. The approximate gradient descent update is given as

$$\boldsymbol{\mu}_{t+1} = \boldsymbol{\mu}_t - \frac{\beta}{n\sigma^2} \sum_{i=1}^n \boldsymbol{\epsilon}_i f(\boldsymbol{\mu}_t + \sigma \boldsymbol{\epsilon}_i), \quad (1)$$

75 where  $\boldsymbol{\epsilon}_i \sim \mathcal{N}(\mathbf{0}, \mathbf{I})$  and  $\beta$  denotes the step-size. The ES method performs the approximate first-order  
 76 gradient descent update. As a result, the convergence of ES may be slow. Several second-order  
 77 gradient descent methods have been proposed to improve convergence. Wierstra et al. [2014a]  
 78 proposed the natural evolution strategies (NES), which perform the approximate natural gradient  
 79 update. When a Gaussian distribution  $\mathcal{N}(\boldsymbol{\mu}, \boldsymbol{\Sigma})$  is employed for sampling. The update rule of NES is  
 80 given in Eq.(2) and Eq.(3):

$$\boldsymbol{\Sigma}_{t+1} = \boldsymbol{\Sigma}_t - \frac{\beta}{n} \sum_{i=1}^n f(\boldsymbol{\mu}_t + \boldsymbol{\Sigma}_t^{\frac{1}{2}} \boldsymbol{\epsilon}_i) \left( \boldsymbol{\Sigma}_t^{\frac{1}{2}} \boldsymbol{\epsilon}_i \boldsymbol{\epsilon}_i^\top \boldsymbol{\Sigma}_t^{\frac{1}{2}} - \boldsymbol{\Sigma}_t \right) \quad (2)$$

$$\boldsymbol{\mu}_{t+1} = \boldsymbol{\mu}_t - \frac{\beta}{n} \sum_{i=1}^n f(\boldsymbol{\mu}_t + \boldsymbol{\Sigma}_t^{\frac{1}{2}} \boldsymbol{\epsilon}_i) \boldsymbol{\Sigma}_t^{\frac{1}{2}} \boldsymbol{\epsilon}_i. \quad (3)$$

81 where  $\epsilon_i \sim \mathcal{N}(\mathbf{0}, \mathbf{I})$  and  $\Sigma_t^{\frac{1}{2}} = \Sigma_t^{\frac{1}{2}\top}$  and  $\Sigma_t^{\frac{1}{2}} \Sigma_t^{\frac{1}{2}} = \Sigma_t$ . The NES takes advantage of second-order  
 82 gradient information, which improves the convergence of ES.

83 Lyu and Tsang [2021] proposed an implicit natural gradient optimizer (INGO) for black-box opti-  
 84 mization, which provides an alternative way to compute the natural gradient update. The update rule  
 85 of INGO is given as in Eq.(5) and Eq.(6):

$$\Sigma_{t+1}^{-1} = \Sigma_t^{-1} + \beta \sum_{i=1}^n \frac{f(\mathbf{x}_i) - \hat{\mu}}{n\hat{\sigma}} (\Sigma_t^{-1}(\mathbf{x}_i - \boldsymbol{\mu}_t)(\mathbf{x}_i - \boldsymbol{\mu}_t)^\top \Sigma_t^{-1} - \Sigma_t^{-1}) \quad (4)$$

$$= \Sigma_t^{-1} + \beta \sum_{i=1}^n \frac{f(\mathbf{x}_i) - \hat{\mu}}{n\hat{\sigma}} (\Sigma_t^{-1}(\mathbf{x}_i - \boldsymbol{\mu}_t)(\mathbf{x}_i - \boldsymbol{\mu}_t)^\top \Sigma_t^{-1}) \quad (5)$$

$$\boldsymbol{\mu}_{t+1} = \boldsymbol{\mu}_t - \beta \sum_{i=1}^n \frac{f(\mathbf{x}_i) - \hat{\mu}}{n\hat{\sigma}} (\mathbf{x}_i - \boldsymbol{\mu}_t). \quad (6)$$

86 where  $\mathbf{x}_i \sim \mathcal{N}(\boldsymbol{\mu}_t, \Sigma_t)$ ,  $\hat{\mu} = \frac{\sum_{i=1}^n f(\mathbf{x}_i)}{n}$  and  $\hat{\sigma}$  denotes the standard deviation of  $f(\mathbf{x}_i)$ . The  
 87 normalization  $\frac{f(\mathbf{x}_i) - \hat{\mu}}{\hat{\sigma}}$  is employed to reduce the variance.

88 CMAES Hansen [2006] provides a more sophisticated update rule and performs well on a wide range  
 89 of black-box optimization problems. All the above stochastic optimization methods rely on sampling.  
 90 Thus, the sampling phase is vitally important. And a better sampling technique is promising to  
 91 achieve further improvement.

## 92 2.2 Rank-1 Lattice

93 A rank-1 lattice is a particular case of the general lattice with a simple operation for point-set  
 94 construction. It can be used as Quasi-Monte Carlo for integral approximation Sloan [2000], Dick  
 95 et al. [2013]. A rank-1 lattice point set  $\mathcal{P} = \{\mathbf{x}_1, \dots, \mathbf{x}_n\}$  can be constructed as Eq.(7):

$$\mathbf{x}_i := \frac{i\mathbf{z} \bmod n}{n}, i \in \{1, \dots, n\}, \quad (7)$$

96 where  $\mathbf{z} \in \mathbb{Z}^d$  is the so-called generating vector, and mod denotes the modulo operation.

97 Korobov [1960] proposes a rank-1 lattice with the generating vector having a particular form as Eq.(8)

$$\mathbf{z} := [1, k, \dots, k^{d-1}] \bmod n, \quad (8)$$

98 where  $k$  is searching over  $\{1, \dots, n-1\}$  to reduce approximation error.

99 Sloan and Reztsov [2002] further proposed a component-by-component searching method for the  
 100 generating vector without assuming the Korobov form in Eq. (8). Recently, Lyu et al. [2020] proposed  
 101 a simple closed-form subgroup-based rank-1 lattice by considering the Toroidal distance in the primal  
 102 lattice space. The generating vector is given as Eq.(9)

$$\mathbf{z} = [g^0, g^{\frac{n-1}{2d}}, g^{\frac{2(n-1)}{2d}}, \dots, g^{\frac{(d-1)(n-1)}{2d}}] \bmod n, \quad (9)$$

103 where  $g$  denotes the primitive root modulo the prime number  $n$ .

104 In this paper, we proposed a closed-form subgroup rank-1 lattice by ensuring the approximation error  
 105 terms of the dual lattice has a more regular pattern. In contrast, Lyu et al. [2020] construct the rank-1  
 106 lattice evenly spaced in the primal lattice space.

## 107 3 Fast Rank-1 Lattice Targeted Sampling

### 108 3.1 Random Rank-1 Lattice Quasi-Monte Carlo Gaussian Sampling

109 We first show how to construct random rank-1 lattice Quasi-Monte Carlo Gaussian samples. These  
 110 samples enable us to perform the black-box stochastic optimization listed in section 2.1. More  
 111 importantly, the nice property of the structure of these samples facilitates a fast targeted sampling.

112 Given a rank-1 lattice point set  $\mathcal{P} = \{\mathbf{x}_1, \dots, \mathbf{x}_n\}$ , we first construct a random shifted rank-1  
 113 lattice Dick et al. [2013] as Eq. (10),

$$\bar{\mathbf{x}}_i = \mathbf{x}_i + \boldsymbol{\Delta} \bmod 1 \quad \forall i \in \{1, \dots, n\}, \quad (10)$$

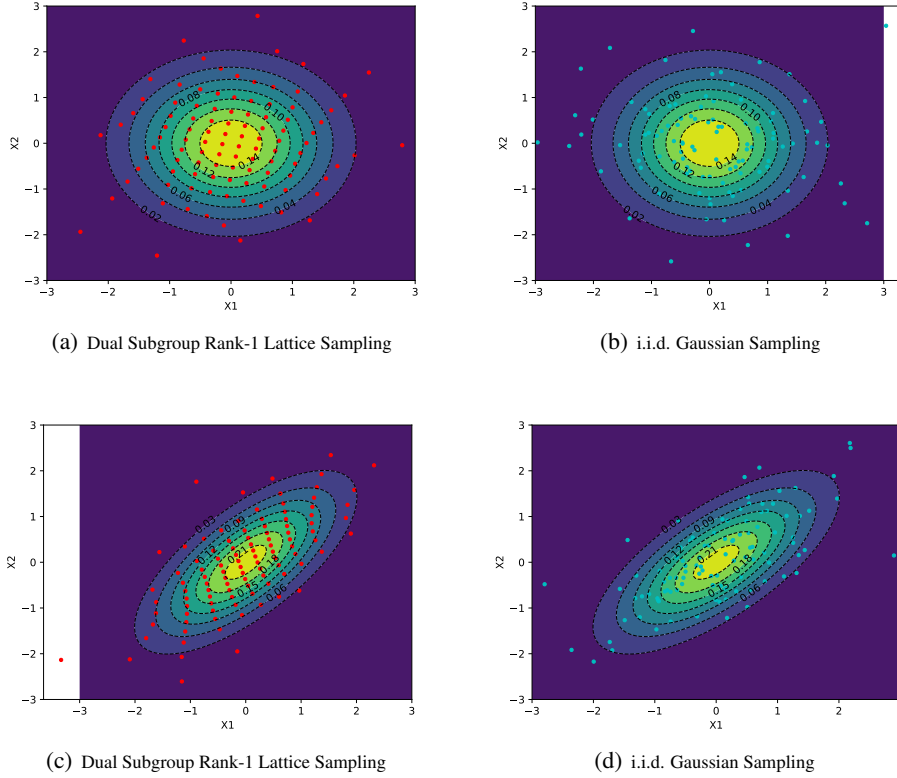


Figure 1: Illustration of the our Dual Subgroup Rank-1 Lattice sampling and i.i.d. Gaussian sampling.

114 where  $\Delta \sim \text{Uniform}[0, 1]^d$ , and the mod 1 operation denotes a modulo operation that takes the  
 115 non-negative fractional part of the input number element-wise. Then, we can construct random QMC  
 116 Gaussian samples as Eq. (11)

$$\epsilon_i = \Phi^{-1}(\bar{x}_i) \quad \forall i \in \{1, \dots, n\}, \quad (11)$$

117 where  $\Phi^{-1}(\cdot)$  computes the inverse cumulative density function of the standard Gaussian distribution  
 118 w.r.t. the input element-wise. Then, the samples for Gaussian  $\mathcal{N}(\mu, \Sigma)$  can be constructed as follows:

$$X_i = \mu + \Sigma^{\frac{1}{2}} \epsilon_i. \quad (12)$$

119 An illustration of the random QMC Gaussian samples constructed by our closed-form rank-1 lattice  
 120 is shown in Figure 1. We can see that our rank-1 lattice QMC Gaussian samples are spaced more  
 121 evenly w.r.t. the density.

### 122 3.2 Fast Exact GP Training and Inference with Rank-1 Lattice

123 This subsection will show how to perform fast exact GP training and inference using our rank-1  
 124 lattice samples with a  $O(n \log n)$  time complexity w.r.t  $n$  samples.

125 Let  $\mathbf{K}_\theta$  denotes the Gram kernel matrix, i.e.,  $\mathbf{K}_\theta = [k_\theta(\mathbf{x}_i, \mathbf{x}_j)]_{1 \leq i, j \leq n}$ , the marginal log-likelihood  
 126 of a GP model Williams and Rasmussen [2006] can be formulated as Eq. (13)

$$\mathcal{L}(p(\mathbf{y}|\mathbf{X})) = -\frac{1}{2} \mathbf{y}^\top (\mathbf{K}_\theta + \sigma^2 \mathbf{I})^{-1} \mathbf{y} - \frac{1}{2} \log(|\mathbf{K}_\theta + \sigma^2 \mathbf{I}|) - \frac{n}{2} \log 2\pi. \quad (13)$$

127 The standard GP model needs a  $O(n^3)$  time complexity to compute the marginal log-likelihood,  
 128 which is prohibitive for fast training as an inner step for stochastic optimization.

129 In this paper, we construct the random QMC samples based on rank-1 lattice, which enables us to  
 130 perform fast GP training. Specifically, we build the GP model with the rank-1 lattice as the training  
 131 data instead of the Gaussian samples. Define modulo kernel as Eq. (14):

$$k(\mathbf{x}_i, \mathbf{x}_j) := k_\Delta(\phi(\mathbf{x}_i - \mathbf{x}_j)), \quad (14)$$

132 where  $k_\Delta(\cdot)$  is a shift-invariant kernel, and the function  $\phi(\mathbf{x}_i - \mathbf{x}_j)$  is given as Eq. (15)

$$\phi(\mathbf{x}_i - \mathbf{x}_j) = \min((\mathbf{x}_i - \mathbf{x}_j) \bmod 1, \mathbf{1} - (\mathbf{x}_i - \mathbf{x}_j) \bmod 1), \quad (15)$$

133 where operation  $\min(\cdot, \cdot)$  outputs the minimum among its two inputs element-wise, and  $\bmod 1$  output  
 134 the positive fractional parts of its inputs element-wise.

135 For a GP model with a modulo kernel defined in Eq.(14), the Gram kernel matrix is a circulant matrix  
 136 thanks to the properties of rank-1 lattice. To be concrete, for rank-1 lattice data, we have Eq.(16)

$$k(\mathbf{x}_i, \mathbf{x}_j) = k(\mathbf{x}_{i+1}, \mathbf{x}_{j+1}) = k_\Delta\left(\min\left(\frac{(i-j)\mathbf{z} \bmod n}{n}, \mathbf{1} - \frac{(i-j)\mathbf{z} \bmod n}{n}\right)\right). \quad (16)$$

137 Then the marginal log-likelihood  $\mathcal{L}(p(\mathbf{y}|\mathbf{X}))$  can be computed with a  $O(n \log n)$  time complexity by  
 138 Fast Fourier Transform. Let  $\mathbf{k}_\Delta^{-1}$  be the shift-invariant kernel vector with elements given as Eq. (17):

$$k_{\Delta i} = k_\Delta\left(\min\left(\frac{(i-1)\mathbf{z} \bmod n}{n}, \mathbf{1} - \frac{(i-1)\mathbf{z} \bmod n}{n}\right)\right), \forall i \in \{1, \dots, n\}. \quad (17)$$

139 Then, we have the fast computation as Eq.(18) and Eq.(19):

$$\mathbf{y}^\top (\mathbf{K}_\theta + \sigma^2 \mathbf{I})^{-1} \mathbf{y} = \mathbf{y}^\top \text{ifft}(\text{fft}(\mathbf{y}) / \text{fft}(\mathbf{k}_\Delta)) \quad (18)$$

$$\log(|\mathbf{K}_\theta + \sigma^2 \mathbf{I}|) = \sum_{i=1}^n \log(\lambda_i + \sigma^2) = \mathbf{1}^\top \text{fft}(\mathbf{k}_\Delta), \quad (19)$$

140 where  $\text{ifft}(\cdot)$ ,  $\text{fft}(\cdot)$  denotes the inverse FFT and FFT operation, respectively, the operator  $/$  in Eq.(18)  
 141 performs divide element-wise. And  $\lambda_i$  in Eq.(19) denotes the eigenvalue of Gram kernel matrix  $\mathbf{K}_\theta$ .

142 For inference, GP model has closed-form posterior mean and variance Williams and Rasmussen  
 143 [2006] given as Eq.(20) and Eq.(21) :

$$\hat{\mathbf{m}}(\mathbf{x}) = \mathbf{k}_\theta(\mathbf{x})^\top (\mathbf{K}_\theta + \sigma^2 \mathbf{I})^{-1} \mathbf{y} \quad (20)$$

$$\hat{\sigma}^2(\mathbf{x}) = k_\theta(\mathbf{x}, \mathbf{x}) - \mathbf{k}_\theta(\mathbf{x})^\top (\mathbf{K}_\theta + \sigma^2 \mathbf{I})^{-1} \mathbf{k}_\theta(\mathbf{x}), \quad (21)$$

144 where  $\mathbf{k}_\theta(\mathbf{x}) = [k_\theta(\mathbf{x}, \mathbf{x}_1), \dots, k_\theta(\mathbf{x}, \mathbf{x}_n)]^\top$ .

145 With rank-1 lattice input data, we can perform fast inference by Eq.(22) and Eq.(23):

$$\hat{\mathbf{m}}(\mathbf{x}) = \mathbf{k}_\theta(\mathbf{x})^\top \text{ifft}(\text{fft}(\mathbf{y}) / \text{fft}(\mathbf{k}_\Delta)) \quad (22)$$

$$\hat{\sigma}^2(\mathbf{x}) = k_\theta(\mathbf{x}, \mathbf{x}) - \mathbf{k}_\theta(\mathbf{x})^\top \text{ifft}(\text{fft}(\mathbf{k}_\theta(\mathbf{x})) / \text{fft}(\mathbf{k}_\Delta)). \quad (23)$$

146 Both the exact GP training and inference benefit from the structure of rank-1 lattice and FFT  
 147 acceleration, which can be performed with a  $O(n \log n)$  time complexity. A deep learning toolbox,  
 148 e.g., Pytorch, can be used to train the parameters of the kernel.

### 149 3.3 Fast Coordinate Search for Targeted Sampling

150 This subsection shows how to perform a fast coordinate search for targeted sampling. A rank-1 lattice  
 151 with  $n$  points is contained in a grid  $\{0, \frac{1}{n}, \dots, \frac{n-1}{n}\}^d$ . We thus perform a coordinate descent search  
 152 from the index set  $\{0, 1, \dots, n-1\}^d$  to minimize the GP posterior mean in Eq.(20).

153 Let  $k(\cdot, \cdot) = k_\Delta(\cdot)$  be a shift-invariant kernel with a decomposition structure as Eq. (24):

$$k(\mathbf{x}^*, \mathbf{x}) = k_\Delta(\phi(\mathbf{x}^* - \mathbf{x})) = \prod_{q=1}^d k_\Delta(\phi(x_q^* - x_q)), \quad (24)$$

---

<sup>1</sup>The element corresponding to  $k_\Delta(\mathbf{0})$  is set to  $k_\Delta(\mathbf{0}) + \sigma^2$ .

---

**Algorithm 1** Fast Coordinate Search
 

---

**Input:** Number of iterations  $T$ , weight vector  $\mathbf{w}$ , and generating vector  $\mathbf{z} = [z_1, \dots, z_d]$  for rank-1 lattice  $\mathbf{X}$ .

**Initialization:** Initialize  $\mathbf{x}^*$  by uniformly sampling from grids  $\{0, \frac{1}{n}, \dots, \frac{n-1}{n}\}^d$ .

**for**  $t=1:T$  **do**

**for**  $q=1:d$  **do**

    Compute  $\mathbf{c}^q = \text{ifft}(\text{fft}(\mathbf{k}_\Delta^q(0)) \odot \text{fft}(\widehat{\mathbf{k}}_\Delta^q \odot \mathbf{w}))$  by Eq.(28).

    Get the index  $i^*$  of the minimum elements in  $\mathbf{c}^q$ , and set  $x_q^* = \frac{i^* z_q \bmod n}{n}$ .

**end for**

**end for**

**Return:**  $\mathbf{x}^*$

---

154 where  $x_q^*, x_q$  denotes the  $q^{\text{th}}$  element in  $\mathbf{x}^*, \mathbf{x}$ , respectively. We can perform a coordinate search by  
 155 fixing all the components except the  $q^{\text{th}}$  one as the current working component for index searching.  
 156 Formally, let  $\mathbf{w} = (\mathbf{K}_\theta + \sigma^2 I)^{-1} \mathbf{y}$ . Then, we have the GP posterior mean function given as Eq. (25):

$$\widehat{m}(\mathbf{x}^*) = \mathbf{k}_\Delta^{q\top}(x_q^*) (\widehat{\mathbf{k}}_\Delta^q \odot \mathbf{w}), \quad (25)$$

157 where  $\odot$  denotes the element-wise product, and  $\mathbf{k}_\Delta^q(x_q^*)$  denotes a vector with  $i^{\text{th}}$  element given as  
 158  $\mathbf{k}_{\Delta i}^q = k_\Delta(\phi(x_q^* - \mathbf{X}_{qi}))$ , and  $\mathbf{X}_{qi}$  denotes the element in  $q^{\text{th}}$ -row and  $i^{\text{th}}$ -column of the rank-1  
 159 lattice matrix  $\mathbf{X} = [\mathbf{x}_1, \dots, \mathbf{x}_n]$ . The vector  $\widehat{\mathbf{k}}_\Delta^q$  denotes the remainder vector with its  $i^{\text{th}}$ -element  
 160 given as Eq. (26):

$$\widehat{\mathbf{k}}_{\Delta i}^q = \frac{1}{k_\Delta(\phi(x_q^* - \mathbf{X}_{qi}))} \prod_{q=1}^d k_\Delta(\phi(x_q^* - \mathbf{X}_{qi})). \quad (26)$$

161 To optimize the  $q^{\text{th}}$  component  $x_q^*$  of  $\mathbf{x}^*$ , we fix the other components of  $\mathbf{x}^*$  and the corresponding  
 162 vector  $\widehat{\mathbf{k}}_\Delta^q$ . We find  $x_q^*$  by solving the subproblem given in Eq. (27)

$$x_q^* = \arg \min_{x \in \{0, \dots, n-1\}} \mathbf{k}_\Delta^q(x)^\top (\widehat{\mathbf{k}}_\Delta^q \odot \mathbf{w}). \quad (27)$$

163 Directly enumerate computation of the problem (27) needs a  $O(n^2)$  time complexity. In our paper,  
 164 we can perform a fast computation with  $O(n \log n)$  time complexity thanks to the rank-1 lattice  
 165  $\mathbf{X}$ . Specially, when  $\mathbf{X}$  is a rank-1 lattice with the generating vector  $\mathbf{z} = [z_1, \dots, z_d]$ , then the  
 166 matrix  $\mathbf{K}_\Delta^q = [\mathbf{k}_\Delta^q(0), \mathbf{k}_\Delta^q(\frac{1z_q \bmod n}{n}), \dots, \mathbf{k}_\Delta^q(\frac{(n-1)z_q \bmod n}{n})]$  forms a circulant matrix, and the  
 167 problem (27) can be accelerated via FFT by Eq. (28)

$$\mathbf{c}^q = \mathbf{K}_\Delta^{q\top} (\widehat{\mathbf{k}}_\Delta^q \odot \mathbf{w}) = \text{ifft}(\text{fft}(\mathbf{k}_\Delta^q(0)) \odot \text{fft}(\widehat{\mathbf{k}}_\Delta^q \odot \mathbf{w})), \quad (28)$$

168 where  $\text{fft}(\cdot)$  and  $\text{ifft}(\cdot)$  denote the FFT and inverse FFT operation. Then, we can achieve  $x_q^*$  by the  
 169 index  $i^*$  of the minimum element in vector  $\mathbf{c}^q = \mathbf{K}_\Delta^{q\top} (\widehat{\mathbf{k}}_\Delta^q \odot \mathbf{w})$ , and set  $x_q^* = \frac{i^* z_q \bmod n}{n}$ .

170 We present the algorithm of the fast coordinate search in Algorithm 1. The Algorithm 1 return a  
 171 targeted sample with a small prediction value in a fast manner. We can use the targeted sample  
 172 to accelerate the stochastic optimization. Finally, we present our overall stochastic optimization  
 173 algorithm in the Algorithm 2. We choose INGO Lyu and Tsang [2021] as our backbone algorithm  
 174 because of its simple implementation and fewer hyperparameters. One can plug our RLTS into other  
 175 stochastic optimization methods to improve query efficiency.

### 176 3.4 Closed-form Rank-1 Lattice Construction

177 This subsection will show how to construct our closed-form dual subgroup rank-1 lattice for fast  
 178 sampling. For  $\forall \mathbf{x}, \mathbf{y} \in [0, 1]^d$  and  $\alpha > 1$ , define a reproducing kernel as Eq. (29)

$$K(\mathbf{x}, \mathbf{y}) = \sum_{\mathbf{k} \in \mathbb{Z}^d} \gamma_\alpha(\mathbf{k}) \exp\left(2\pi i \mathbf{k}^\top (\mathbf{x} - \mathbf{y})\right), \quad (29)$$

---

**Algorithm 2** Rank-1 Lattice Targeted Sampling
 

---

**Input:** Number of Samples  $n$ , step-size  $\beta$  and  $\eta$ , number of internal iterations  $T$  for Fast Coordinate Search, and initial variance  $\sigma^2$ .

**Initialization:** Initialize  $\boldsymbol{\mu}_0 = \mathbf{0}$  and  $\boldsymbol{\Sigma}_0 = \sigma^2 \mathbf{I}$ .

**while** Termination condition not satisfied **do**

  Sample a shift vector  $\Delta$  uniformly from  $[0, 1]^d$ .

  Construct shifted rank-1 lattice  $\bar{\mathbf{X}} = [\bar{\mathbf{x}}_1, \dots, \bar{\mathbf{x}}_n]$  by Eq.(10).

  Construct QMC Gaussian Samples  $\boldsymbol{\epsilon}_1, \dots, \boldsymbol{\epsilon}_n$  by Eq.(11).

  Set  $\mathbf{x}_i = \boldsymbol{\mu}_t + \boldsymbol{\Sigma}_t^{\frac{1}{2}} \boldsymbol{\epsilon}_i$  for  $i \in \{1, \dots, n\}$ .

  Query the batch observations  $\{f(\mathbf{x}_1), \dots, f(\mathbf{x}_n)\}$

  Compute  $\hat{\sigma} = \text{std}(f(\mathbf{x}_1), \dots, f(\mathbf{x}_n))$ .

  Compute  $\hat{\boldsymbol{\mu}} = \frac{1}{n} \sum_{i=1}^n f(\mathbf{x}_i)$ .

  Set  $y_i = \frac{f(\mathbf{x}_i) - \hat{\boldsymbol{\mu}}}{\hat{\sigma}}$  for  $i \in \{1, \dots, n\}$ .

  Perform fast exact GP training with rank-1 lattice  $\bar{\mathbf{X}}$  and  $\mathbf{y}$  by Eq.(18) and Eq.(19).

  Get targeted grid sample  $\bar{\mathbf{x}}^*$  by Algorithm 1 with  $T$  steps.

  Get targeted Gaussian sample  $\mathbf{x}^* = \Phi^{-1}(\bar{\mathbf{x}}^* + \Delta \bmod 1)$

  Query the observation  $f(\mathbf{x}^*)$ .

  Set  $\boldsymbol{\Sigma}_{t+1}^{-1} = \boldsymbol{\Sigma}_t^{-1} + \frac{\beta}{n} \sum_{i=1}^n y_i \boldsymbol{\Sigma}_t^{-\frac{1}{2}} \boldsymbol{\epsilon}_i \boldsymbol{\epsilon}_i^\top \boldsymbol{\Sigma}_t^{-\frac{1}{2}}$ .

  Set  $\boldsymbol{\mu}_{t+1} = \boldsymbol{\mu}_t - \frac{\beta}{n} \sum_{i=1}^n y_i \boldsymbol{\Sigma}_t^{\frac{1}{2}} \boldsymbol{\epsilon}_i$

**if**  $f(\mathbf{x}^*) < \min_{i \in \{1, \dots, n\}} f(\mathbf{x}_i)$  **then**

    Set  $\boldsymbol{\mu}_{t+1} = (1 - \eta)\boldsymbol{\mu}_{t+1} + \eta\mathbf{x}^*$

**end if**

**end while**

---

179 where  $\mathbf{i}^2 = -1$  and  $\gamma_\alpha(\mathbf{k}) = \prod_{j=1}^d \gamma_\alpha(k_j)$  with  $\gamma_\alpha(k)$  is given as follows:

$$\gamma_\alpha(k) = \begin{cases} 1 & \text{if } k = 0 \\ |k|^{-\alpha} & \text{if } k \neq 0. \end{cases} \quad (30)$$

180 The reproducing kernel Hilbert space (RKHS) associated with the kernel in Eq.(29) is a Korobov  
181 space, denoted as  $\mathcal{H}_k$ . Our closed form of the generating vector is given as Eq.(31):

$$\mathbf{z} = [g^0, g^{\frac{n-1}{2d-1}}, g^{\frac{2(n-1)}{2d-1}}, \dots, g^{\frac{(d-1)(n-1)}{2d-1}}] \bmod n, \quad (31)$$

182 where  $g$  denotes the primitive root modulo the prime number  $n$ , and  $(2d-1)|(n-1)$ . Then, our dual  
183 subgroup rank-1 lattice can be achieved by Eq. (7)

184 Given a point set  $\mathcal{P} = \{\mathbf{x}_1, \dots, \mathbf{x}_n\}$ , the square worst case integral approximation error for  $f \in \mathcal{H}_k$   
185 is defined as Eq.(32):

$$e^2(\mathcal{H}_k; \mathcal{P}) = \sup_{f \in \mathcal{H}_k, \|f\|_{\mathcal{H}_k} \leq 1} \left| \int_{[0,1]^d} f(\mathbf{x}) d\mathbf{x} - \frac{1}{n} \sum_{j=0}^{n-1} f(\mathbf{x}_j) \right|^2. \quad (32)$$

186 We further show that our rank-1 lattice constructed by Eq. (31) has a regular worst-case error pattern  
187 in Theorem 1. The proof is given in the Appendix.

188 **Theorem 1.** *Let  $n$  be a prime number such that  $(2d-1)|(n-1)$ . Suppose the integrand function*  
189  *$f \in \mathcal{H}_k$ ,  $\|f\|_{\mathcal{H}_k} \leq 1$ , the square worst-case integral approximation error of rank-1 lattice  $\mathcal{P}$*   
190 *constructed by Eq.(31) is given as Eq.(33):*

$$e^2(\mathcal{H}_k; \mathcal{P}) = \frac{1}{2n} \mathbf{1}^\top (\mathbf{h}^0 \odot \dots \odot \mathbf{h}^{2d-2} - 1 - (\mathbf{h}^1 \odot \dots \odot \mathbf{h}^{d-1} - 1) \odot \mathbf{h}^0 \odot (\mathbf{h}^{-1} \odot \dots \odot \mathbf{h}^{-(d-1)} - 1)) + \frac{1}{n^\alpha} \zeta(\alpha, 1), \quad (33)$$

191 where  $\odot$  denotes the element-wise product, symbol  $\mathbf{1}$  denotes the vector with elements all ones,  
192 and  $\mathbf{h}^i = \mathbf{F}^i \boldsymbol{\gamma}$  with  $\mathbf{F}$  as the discrete Fourier matrix, i.e.,  $\mathbf{F}_{jk} = \exp(2\pi i \frac{jk}{n})$ , and  $\mathbf{F}^i$  denotes  
193 the matrix after permutation of the rows of  $\mathbf{F}$  such that the  $j^{\text{th}}$  row of  $\mathbf{F}^i$  equals to the  $\tilde{j}^{\text{th}}$  row of  
194  $\mathbf{F}$ , where  $\tilde{j} = jg^{\frac{i(n-1)}{2d-1}} \bmod n$ . And  $\boldsymbol{\gamma} = [\gamma_1, \dots, \gamma_n]^\top$  with  $\gamma_k = \frac{1}{n^\alpha} (\zeta(\alpha, \frac{k_i}{n}) + \zeta(\alpha, \frac{n-k_i}{n}))$  for  
195  $k \in \{1, \dots, n-1\}$  and  $\gamma_n = 1 + \frac{2}{n^\alpha} \zeta(\alpha, 1)$ , where  $\zeta(\cdot, \cdot)$  denotes the Hurwitz zeta function.

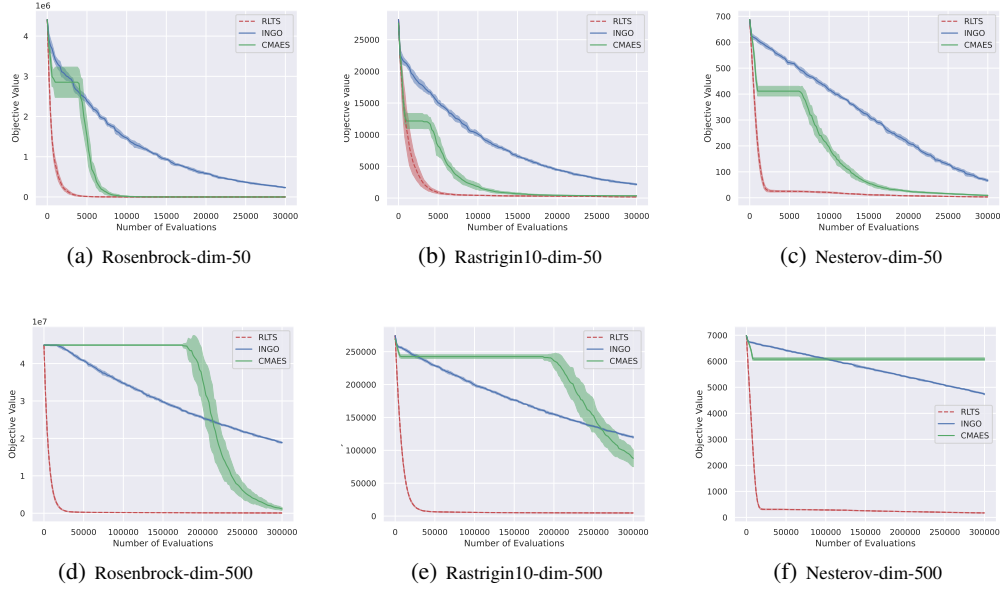


Figure 2: Cumulative min objective value v.s. the number of queries on 50-dimensional and 500-dimensional benchmark test functions.

196 **Remarks:** The term  $H = \mathbf{h}^0 \odot \dots \odot \mathbf{h}^{2d-2} - \mathbf{1} - (\mathbf{h}^1 \odot \dots \odot \mathbf{h}^{d-1} - \mathbf{1}) \odot \mathbf{h}^0 \odot (\mathbf{h}^{-1} \odot \dots \odot \mathbf{h}^{-(d-1)} - \mathbf{1})$   
197 has a regular pattern because of  $\{g^0, g^{\frac{n-1}{2d-1}}, g^{\frac{2(n-1)}{2d-1}}, \dots, g^{\frac{(d-1)(n-1)}{2d-1}}, \dots, g^{\frac{(2d-2)(n-1)}{2d-1}}\} \bmod n$   
198 forms a subgroup of  $\{1, \dots, n-1\} \bmod n$ . According to the Lagrange's theorem in group  
199 theory Dummit and Foote [2004], the vector  $\mathbf{h}^0 \odot \dots \odot \mathbf{h}^{2d-2}$  has  $\frac{n-1}{2d-1}$  different elements.

## 200 4 Experiments

201 We replace the i.i.d. Gaussian sampling of the INGO Lyu and Tsang [2021] with our RLTS. We  
202 evaluate our RLTS by comparing it with the standard INGO and the CMAES Hansen [2006]. In  
203 all the experiments, we keep the number of batch samples and the initialization the same for RLTS,  
204 INGO and CMAES. For all the methods, we initialize the  $\boldsymbol{\mu} = \mathbf{0}$ . For INGO and RLTS, we set  
205 the step-size parameter  $\beta = 0.2$  in all experiments. For RLTS, we set the parameter  $\eta = 1$  in all  
206 experiments.

### 207 4.1 Evaluation on Benchmark Functions

208 We first evaluate our RLTS on challenging benchmark test functions: Rosenbrock, Rastrigin, and  
209 Nesterov. Rastrigin and Rosenbrock are smooth multi-mode functions, and Nesterov is a non-smooth  
210 function. These functions are very challenging benchmarks for black-box optimization. We offset the  
211 optimum by setting  $\mathbf{x} = \mathbf{x} - 5$  of the test functions. This increases the distance between the optimum  
212 and the initial point  $\mathbf{0}$ , which makes the test problems more challenging. We implement INGO by  
213 ourselves. For CMAES, we use the publicly available code <sup>2</sup>

214 We evaluate RLTS on 50 and 500-dimensional problems. All the experiments are performed in ten  
215 independent runs. The experimental results are shown in Figure 2. From Figure 2, we can observe that  
216 RLTS consistently converge faster than INGO on all the test functions on both 50-dimensional and  
217 500-dimensional cases. It shows that our RLTS significantly improves the query efficiency of INGO,  
218 which verifies the effectiveness of RLTS. Moreover, we can see that RLTS outperforms CMAES on  
219 all the test functions on both 50-dimensional and 500-dimensional cases. In addition, we see that  
220 CMAES converge slowly on the 500-dimensional benchmark problems, while RLTS converges faster.

<sup>2</sup><https://pypi.org/project/cma/>



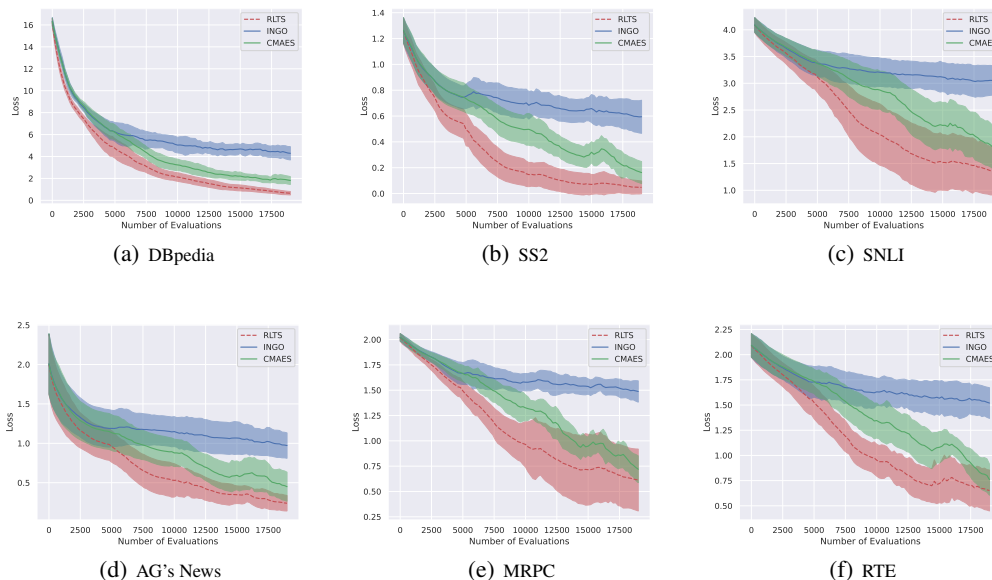


Figure 3: Hinge loss v.s. the number of queries on different black-box fine-tuning models.

## 221 4.2 Evaluation on Black-box Prompt Fine-tuning Tasks

222 The great success of ChatGPT shows the promising potential of large language models. Prompt  
 223 fine-tuning of large language models is a promising direction to achieve expertise models efficiently  
 224 for downstream tasks. We further evaluate our RLTS on black-box prompt fine-tuning tasks.

225 We employ the publicly available code <sup>3</sup> as the backbone model of black-box prompt fine-tuning.  
 226 We employ the hinge loss of the training set as the black-box objective. Six benchmark datasets  
 227 for different language tasks are employed for evaluation: DBpedia, SS2, SNLI, AG’s News, MRPC  
 228 and RTE. The SST2 Socher et al. [2013] dataset is a dataset for the sentiment analysis task. AG’s  
 229 News and DBpedia datasets Zhang et al. [2015] are used for topic classification tasks. SNLI Bowman  
 230 et al. [2015] and RTE Wang et al. [2019] are employed for natural language inference. MRPC  
 231 dataset Dolan and Brockett [2005] is used for the paraphrasing task.

232 The dimension of the continuous prompt is set to  $24 \times 50$ . All the experiments are performed in five  
 233 independent runs with seeds in  $\{1, 2, 3, 4, 5\}$ . The experimental results are shown in Figure 3. From  
 234 Figure 3, we can observe that RLTS decreases the loss consistently faster than INGO and CMAES on  
 235 all benchmark datasets. More importantly, RLTS decreases the loss significantly faster than INGO.  
 236 Note that RLTS employs INGO as the backbone algorithm, which shows that RLTS improves the  
 237 query efficiency of INGO. More experimental results can be found in the Appendix.

## 238 5 Conclusion

239 We proposed a novel Rank-1 Lattice Targeted Sampling technique in this paper. Our RLTS has  
 240 a  $O(n \log n)$  time complexity w.r.t.  $n$  batch samples, which is fast for plugging into stochastic  
 241 optimization methods to improve query efficiency while scaling up to high-dimensional problems.  
 242 Empirically, we plugged our RLTS into the sampling phase of INGO, significantly improving the  
 243 query efficiency on benchmark test functions and black-box prompt fine-tuning tasks. Moreover, we  
 244 proposed a closed-form rank-1 lattice by analyzing the integral approximation error of functions in  
 245 Korobov space. Our closed-form rank-1 lattice provides an efficient way for QMC Gaussian sampling,  
 246 with properties enabling fast exact GP training and inference with a  $O(n \log n)$  time complexity,  
 247 which is critical for our RLTS to be a fast internal step for stochastic optimization. In addition, our  
 248 closed-form rank-1 lattice is a fundamental tool that may have potential applications beyond the  
 249 black-box optimization task.

<sup>3</sup><https://github.com/txsun1997/Black-Box-Tuning>

## 250 References

- 251 Thomas Back, Frank Hoffmeister, and Hans-Paul Schwefel. A survey of evolution strategies. In  
252 *Proceedings of the fourth international conference on genetic algorithms*, volume 2. Morgan  
253 Kaufmann Publishers San Mateo, CA, 1991.
- 254 Juan Cruz Barsce, Jorge A Palombarini, and Ernesto C Martínez. Towards autonomous reinforcement  
255 learning: Automatic setting of hyper-parameters using bayesian optimization. In *Computer*  
256 *Conference (CLEI), 2017 XLIII Latin American*, pages 1–9. IEEE, 2017.
- 257 Samuel R Bowman, Gabor Angeli, Christopher Potts, and Christopher D Manning. A large annotated  
258 corpus for learning natural language inference. *Proceedings of the 2015 conference on empirical*  
259 *methods in natural language processing*, 2015.
- 260 Krzysztof Choromanski, Aldo Pacchiano, Jack Parker-Holder, and Yunhao Tang. From complexity to  
261 simplicity: Adaptive es-active subspaces for blackbox optimization. *arXiv:1903.04268*, 2019.
- 262 Josef Dick, Frances Y Kuo, and Ian H Sloan. High-dimensional integration: the quasi-monte carlo  
263 way. *Acta Numerica*, 22:133–288, 2013.
- 264 Bill Dolan and Chris Brockett. Automatically constructing a corpus of sentential paraphrases. In  
265 *Third International Workshop on Paraphrasing (IWP2005)*, 2005.
- 266 David Steven Dummit and Richard M Foote. *Abstract algebra*, volume 3. Wiley Hoboken, 2004.
- 267 David Eriksson, Michael Pearce, Jacob Gardner, Ryan D Turner, and Matthias Poloczek. Scalable  
268 global optimization via local bayesian optimization. *Advances in neural information processing*  
269 *systems*, 32, 2019.
- 270 Jacob Gardner, Chuan Guo, Kilian Weinberger, Roman Garnett, and Roger Grosse. Discovering and  
271 exploiting additive structure for bayesian optimization. In *Artificial Intelligence and Statistics*,  
272 pages 1311–1319. PMLR, 2017.
- 273 Nikolaus Hansen. The cma evolution strategy: a comparing review. In *Towards a new evolutionary*  
274 *computation*, pages 75–102. Springer, 2006.
- 275 José Miguel Hernández-Lobato, James Requeima, Edward O Pyzer-Knapp, and Alán Aspuru-Guzik.  
276 Parallel and distributed thompson sampling for large-scale accelerated exploration of chemical  
277 space. In *International conference on machine learning*, pages 1470–1479. PMLR, 2017.
- 278 Nikolai Mikhailovich Korobov. Properties and calculation of optimal coefficients. In *Doklady*  
279 *Akademii Nauk*, volume 132, pages 1009–1012. Russian Academy of Sciences, 1960.
- 280 Daniel J Lizotte, Tao Wang, Michael H Bowling, and Dale Schuurmans. Automatic gait optimization  
281 with gaussian process regression. In *IJCAI*, volume 7, pages 944–949, 2007.
- 282 Yueming Lyu and Ivor W Tsang. Black-box optimizer with stochastic implicit natural gradient. In  
283 *Machine Learning and Knowledge Discovery in Databases. Research Track: European Conference,*  
284 *ECML PKDD 2021, Bilbao, Spain, September 13–17, 2021, Proceedings, Part III 21*, pages  
285 217–232. Springer, 2021.
- 286 Yueming Lyu, Yuan Yuan, and Ivor Tsang. Subgroup-based rank-1 lattice quasi-monte carlo. *Ad-*  
287 *vances in Neural Information Processing Systems*, 33:6269–6280, 2020.
- 288 Wesley Maddox, Qing Feng, and Max Balandat. Optimizing high-dimensional physics simulations  
289 via composite bayesian optimization. *arXiv preprint arXiv:2111.14911*, 2021.
- 290 Seyedali Mirjalili and Seyedali Mirjalili. Genetic algorithm. *Evolutionary Algorithms and Neural*  
291 *Networks: Theory and Applications*, pages 43–55, 2019.
- 292 Sarah Müller, Alexander von Rohr, and Sebastian Trimpe. Local policy search with bayesian  
293 optimization. *Advances in Neural Information Processing Systems*, 34:20708–20720, 2021.
- 294 Amin Nayebi, Alexander Munteanu, and Matthias Poloczek. A framework for bayesian optimization  
295 in embedded subspaces. In *International Conference on Machine Learning*, pages 4752–4761.  
296 PMLR, 2019.

- 297 Diana M Negoescu, Peter I Frazier, and Warren B Powell. The knowledge-gradient algorithm for  
298 sequencing experiments in drug discovery. *INFORMS Journal on Computing*, 23(3):346–363,  
299 2011.
- 300 Yurii Nesterov and Vladimir Spokoiny. Random gradient-free minimization of convex functions.  
301 *Foundations of Computational Mathematics*, 17(2):527–566, 2017.
- 302 Quan Nguyen, Kaiwen Wu, Jacob Gardner, and Roman Garnett. Local bayesian optimization  
303 via maximizing probability of descent. *Advances in neural information processing systems*, 35:  
304 13190–13202, 2022.
- 305 Ingo Rechenberg and M. Eigen. *Optimierung technischer Systeme nach Prinzipien der biologischen*  
306 *Evolution*. PhD thesis, 1973.
- 307 Tim Salimans, Jonathan Ho, Xi Chen, Szymon Sidor, and Ilya Sutskever. Evolution strategies as a  
308 scalable alternative to reinforcement learning. *arXiv preprint arXiv:1703.03864*, 2017.
- 309 I Sloan and A Reztsov. Component-by-component construction of good lattice rules. *Mathematics of*  
310 *Computation*, 71(237):263–273, 2002.
- 311 Ian H Sloan. Multiple integration is intractable but not hopeless. *The ANZIAM Journal*, 42(1):3–8,  
312 2000.
- 313 Jasper Snoek, Hugo Larochelle, and Ryan P Adams. Practical bayesian optimization of machine  
314 learning algorithms. In *NeurIPS*, pages 2951–2959, 2012.
- 315 Richard Socher, Alex Perelygin, Jean Wu, Jason Chuang, Christopher D Manning, Andrew Y Ng, and  
316 Christopher Potts. Recursive deep models for semantic compositionality over a sentiment treebank.  
317 In *Proceedings of the 2013 conference on empirical methods in natural language processing*, pages  
318 1631–1642, 2013.
- 319 Mandavilli Srinivas and Lalit M Patnaik. Genetic algorithms: A survey. *computer*, 27(6):17–26,  
320 1994.
- 321 Niranjan Srinivas, Andreas Krause, Sham M Kakade, and Matthias Seeger. Gaussian process  
322 optimization in the bandit setting: No regret and experimental design. In *ICML*, 2010.
- 323 Tianxiang Sun, Zhengfu He, Hong Qian, Yunhua Zhou, Xuanjing Huang, and Xipeng Qiu. Bbtv2:  
324 Towards a gradient-free future with large language models. In *Proceedings of EMNLP*, 2022a.
- 325 Tianxiang Sun, Yunfan Shao, Hong Qian, Xuanjing Huang, and Xipeng Qiu. Black-box tuning for  
326 language-model-as-a-service. In *Proceedings of ICML*, 2022b.
- 327 Alex Wang, Amanpreet Singh, Julian Michael, Felix Hill, Omer Levy, and Samuel R Bowman.  
328 Glue: A multi-task benchmark and analysis platform for natural language understanding. In *7th*  
329 *International Conference on Learning Representations, ICLR*, 2019.
- 330 G Gary Wang and Songqing Shan. Review of metamodeling techniques in support of engineering  
331 design optimization. *Journal of Mechanical design*, 129(4):370–380, 2007.
- 332 Daan Wierstra, Tom Schaul, Tobias Glasmachers, Yi Sun, Jan Peters, and Jürgen Schmidhuber.  
333 Natural evolution strategies. *The Journal of Machine Learning Research (JMLR)*, 15(1):949–980,  
334 2014a.
- 335 Daan Wierstra, Tom Schaul, Tobias Glasmachers, Yi Sun, Jan Peters, and Jürgen Schmidhuber.  
336 Natural evolution strategies. *The Journal of Machine Learning Research*, 15(1):949–980, 2014b.
- 337 Christopher KI Williams and Carl Edward Rasmussen. *Gaussian processes for machine learning*,  
338 volume 2. MIT press Cambridge, MA, 2006.
- 339 Xiang Zhang, Junbo Zhao, and Yann LeCun. Character-level convolutional networks for text  
340 classification. *Advances in neural information processing systems*, 28, 2015.

## 341 A Proof of Theorem 1

342 We provide an improved Theorem 1 in the current version, which builds an improved result regarding  
343 the exact error  $e^2(\mathcal{H}_k; \mathcal{P})$  instead of the asymptotic order in the previous version.

344 **Theorem 1.** *Let  $n$  be a prime number such that  $(2d-1)|(n-1)$ . Suppose the integrand function  
345  $f \in \mathcal{H}_k, \|f\|_{\mathcal{H}_k} \leq 1$ , the square worst-case integral approximation error of rank-1 lattice  $\mathcal{P}$   
346 constructed by Eq.(31) is given as Eq.(34):*

$$e^2(\mathcal{H}_k; \mathcal{P}) = \frac{1}{2^n} \mathbf{1}^\top (\mathbf{h}^0 \odot \dots \odot \mathbf{h}^{2d-2} - \mathbf{1} - (\mathbf{h}^1 \odot \dots \odot \mathbf{h}^{d-1} - \mathbf{1}) \odot \mathbf{h}^0 \odot (\mathbf{h}^{-1} \odot \dots \odot \mathbf{h}^{-(d-1)} - \mathbf{1})) + \frac{1}{n^\alpha} \zeta(\alpha, 1), \quad (34)$$

347 where  $\odot$  denotes the element-wise product, symbol  $\mathbf{1}$  denotes the vector with elements all ones,  
348 and  $\mathbf{h}^i = \mathbf{F}^i \boldsymbol{\gamma}$  with  $\mathbf{F}$  as the discrete Fourier matrix, i.e.,  $\mathbf{F}_{jk} = \exp(2\pi i \frac{jk}{n})$ , and  $\mathbf{F}^i$  denotes  
349 the matrix after permutation of the rows of  $\mathbf{F}$  such that the  $j^{\text{th}}$  row of  $\mathbf{F}^i$  equals to the  $\tilde{j}^{\text{th}}$  row of  
350  $\mathbf{F}$ , where  $\tilde{j} = jg^{\frac{i(n-1)}{2d-1}} \bmod n$ . And  $\boldsymbol{\gamma} = [\gamma_1, \dots, \gamma_n]^\top$  with  $\gamma_k = \frac{1}{n^\alpha} (\zeta(\alpha, \frac{k_i}{n}) + \zeta(\alpha, \frac{n-k_i}{n}))$  for  
351  $k \in \{1, \dots, n-1\}$  and  $\gamma_n = 1 + \frac{2}{n^\alpha} \zeta(\alpha, 1)$ , where  $\zeta(\cdot, \cdot)$  denotes the Hurwitz zeta function.

352 To prove our main Theorem 1, we begin with several Lemma.

353 **Lemma 1.** *For  $\forall \mathbf{x}, \mathbf{y} \in [0, 1]^d$  and  $\alpha > 1$ , define a reproducing kernel as Eq.(35)*

$$K(\mathbf{x}, \mathbf{y}) = \sum_{\mathbf{k} \in \mathbb{Z}^d} \gamma_\alpha(\mathbf{k}) \exp\left(2\pi i \mathbf{k}^\top (\mathbf{x} - \mathbf{y})\right), \quad (35)$$

354 where  $\gamma_\alpha(\mathbf{k}) = \prod_{j=1}^d \gamma_\alpha(k_j)$  with  $\gamma_\alpha(k)$  given in Eq.(36)

$$\gamma_\alpha(k) = \begin{cases} 1 & \text{if } k = 0 \\ |k|^{-\alpha} & \text{if } k \neq 0. \end{cases} \quad (36)$$

355 Let  $\mathcal{P} = [\mathbf{x}_1, \dots, \mathbf{x}_n]$  be a rank-1 lattice constructed by the generating vector  $\mathbf{z}$  with a prime number  
356  $n$ . Then, for  $\forall f \in \mathcal{H}_k, \|f\|_{\mathcal{H}_k} \leq 1$  associated with the reproducing kernel Eq.(35), we have the  
357 square worst-case integral approximation error of  $\mathcal{P}$  as Eq.(37).

$$e^2(\mathcal{H}_k; \mathcal{P}) = \sup_{f \in \mathcal{H}_k, \|f\|_{\mathcal{H}_k} \leq 1} \left| \int_{[0,1]^d} f(\mathbf{x}) d\mathbf{x} - \frac{1}{n} \sum_{j=0}^{n-1} f(\mathbf{x}_j) \right|^2 = \sum_{\mathbf{k} \in L^\perp \setminus \{\mathbf{0}\}} \gamma_\alpha(\mathbf{k}) \quad (37)$$

358 where  $L^\perp$  denote the dual lattice defined in Eq.(38).

$$L^\perp := \{\mathbf{k} | \mathbf{k}^\top \mathbf{z} \equiv 0 \pmod{n}, \mathbf{k} \in \mathbb{Z}^d\}. \quad (38)$$

359 *Proof.* Given a point set  $\mathcal{P} = \{\mathbf{x}_1, \dots, \mathbf{x}_n\}$ , the worst case approximation error for  $\forall f \in$   
360  $\mathcal{H}_k, \|f\|_{\mathcal{H}_k} \leq 1$  is

$$e^2(\mathcal{H}_k; \mathcal{P}) = \sup_{f \in \mathcal{H}_k, \|f\|_{\mathcal{H}_k} \leq 1} \left| \int_{[0,1]^d} f(\mathbf{x}) d\mathbf{x} - \frac{1}{n} \sum_{j=0}^{n-1} f(\mathbf{x}_j) \right|^2 \quad (39)$$

$$= \sup_{f \in \mathcal{H}_k, \|f\|_{\mathcal{H}_k} \leq 1} \left| \left\langle f, \int_{[0,1]^d} K(\mathbf{x}, \cdot) d\mathbf{x} - \frac{1}{n} \sum_{j=0}^{n-1} K(\mathbf{x}_j, \cdot) \right\rangle_{\mathcal{H}_k} \right|^2 \quad (40)$$

$$= \sup_{f \in \mathcal{H}_k, \|f\|_{\mathcal{H}_k} \leq 1} \|f\|_{\mathcal{H}_k} \left\| \int_{[0,1]^d} K(\mathbf{x}, \cdot) d\mathbf{x} - \frac{1}{n} \sum_{j=0}^{n-1} K(\mathbf{x}_j, \cdot) \right\|_{\mathcal{H}_k} \quad (41)$$

$$= \int_{[0,1]^d} \int_{[0,1]^d} K(\mathbf{x}, \mathbf{y}) d\mathbf{x} d\mathbf{y} - \frac{2}{n} \sum_{j=1}^n \int_{[0,1]^d} K(\mathbf{x}, \mathbf{x}_j) d\mathbf{x} + \frac{1}{n^2} \sum_{i,j=1}^n K(\mathbf{x}_i, \mathbf{x}_j) \quad (42)$$

361 Then, from the definition of the reproducing kernel  $K(\mathbf{x}, \mathbf{y})$  in Eq.(35), we know that

$$\int_{[0,1]^d} \int_{[0,1]^d} K(\mathbf{x}, \mathbf{y}) d\mathbf{x} d\mathbf{y} = \int_{[0,1]^d} \int_{[0,1]^d} \sum_{\mathbf{k} \in \mathbb{Z}^d} \gamma_\alpha(\mathbf{k}) \exp\left(2\pi i \mathbf{k}^\top (\mathbf{x} - \mathbf{y})\right) d\mathbf{x} d\mathbf{y} \quad (43)$$

$$= 1 + \sum_{\mathbf{k} \in \mathbb{Z}^d, \mathbf{k} \neq \mathbf{0}} \gamma_\alpha(\mathbf{k}) \int_{[0,1]^d} \int_{[0,1]^d} \exp\left(2\pi i \mathbf{k}^\top (\mathbf{x} - \mathbf{y})\right) d\mathbf{x} d\mathbf{y} \quad (44)$$

$$= 1 + \sum_{\mathbf{k} \in \mathbb{Z}^d, \mathbf{k} \neq \mathbf{0}} \gamma_\alpha(\mathbf{k}) \cdot 0 = 1 \quad (45)$$

362 In addition, the second term in Eq.(42) as follows

$$- \frac{2}{n} \sum_{j=1}^n \int_{[0,1]^d} K(\mathbf{x}, \mathbf{x}_j) d\mathbf{x} \quad (46)$$

$$= - \frac{2}{n} \sum_{j=1}^n \int_{[0,1]^d} \sum_{\mathbf{k} \in \mathbb{Z}^d} \gamma_\alpha(\mathbf{k}) \exp\left(2\pi i \mathbf{k}^\top (\mathbf{x} - \mathbf{x}_j)\right) d\mathbf{x} \quad (47)$$

$$= - \frac{2}{n} \sum_{j=1}^n \gamma_\alpha(\mathbf{0}) - \frac{2}{n} \sum_{j=1}^n \sum_{\mathbf{k} \in \mathbb{Z}^d, \mathbf{k} \neq \mathbf{0}} \gamma_\alpha(\mathbf{k}) \int_{[0,1]^d} \exp\left(2\pi i \mathbf{k}^\top (\mathbf{x} - \mathbf{x}_j)\right) d\mathbf{x} \quad (48)$$

$$= - \frac{2}{n} \sum_{j=1}^n \gamma_\alpha(\mathbf{0}) - \frac{2}{n} \sum_{j=1}^n \sum_{\mathbf{k} \in \mathbb{Z}^d, \mathbf{k} \neq \mathbf{0}} \gamma_\alpha(\mathbf{k}) \cdot 0 \quad (49)$$

$$= -2 \quad (50)$$

363 Moreover, from the definition of rank-1 lattice  $\mathcal{P}$  with prime  $n$  and generating vector  $\mathbf{z}$ , we have the  
364 third term in Eq.(42) as follows

$$\frac{1}{n^2} \sum_{i,j=1}^n K(\mathbf{x}_i, \mathbf{x}_j) \quad (51)$$

$$= \frac{1}{n^2} \sum_{i,j=1}^n \sum_{\mathbf{k} \in \mathbb{Z}^d} \gamma_\alpha(\mathbf{k}) \exp\left(2\pi i \mathbf{k}^\top (\mathbf{x}_i - \mathbf{x}_j)\right) \quad (52)$$

$$= 1 + \frac{1}{n^2} \sum_{i,j=1}^n \sum_{\mathbf{k} \in \mathbb{Z}^d, \mathbf{k} \neq \mathbf{0}} \gamma_\alpha(\mathbf{k}) \exp\left(\frac{2\pi i (i-j) \mathbf{k}^\top \mathbf{z}}{n}\right) \quad (53)$$

$$= 1 + \sum_{\mathbf{k} \in \mathbb{Z}^d, \mathbf{k} \neq \mathbf{0}} \gamma_\alpha(\mathbf{k}) \frac{1}{n^2} \sum_{i,j=1}^n \exp\left(\frac{2\pi i (i-j) \mathbf{k}^\top \mathbf{z}}{n}\right) \quad (54)$$

$$= 1 + \sum_{\mathbf{k} \in \mathbb{Z}^d, \mathbf{k} \neq \mathbf{0}} \gamma_\alpha(\mathbf{k}) \frac{1}{n} \sum_{j=1}^n \exp\left(\frac{2\pi i j \mathbf{k}^\top \mathbf{z}}{n}\right) \quad (55)$$

365 Put Eq.(45), Eq.(50) and Eq.(55) together, we know that

$$e^2(\mathcal{H}_k; \mathcal{P}) = \sum_{\mathbf{k} \in \mathbb{Z}^d, \mathbf{k} \neq \mathbf{0}} \gamma_\alpha(\mathbf{k}) \frac{1}{n} \sum_{j=1}^n \exp\left(\frac{2\pi i j \mathbf{k}^\top \mathbf{z}}{n}\right) \quad (56)$$

366 Note that for a prime number  $n$ , we have

$$\frac{1}{n} \sum_{j=1}^n \exp\left(\frac{2\pi i j \mathbf{k}^\top \mathbf{z}}{n}\right) = \begin{cases} 1 & \text{if } \mathbf{k}^\top \mathbf{z} \equiv 0 \pmod{n} \\ 0 & \text{otherwise} \end{cases} \quad (57)$$

367 It follows that

$$e^2(\mathcal{H}_k; \mathcal{P}) = \sup_{f \in \mathcal{H}_k, \|f\|_{\mathcal{H}_k} \leq 1} \left| \int_{[0,1]^d} f(\mathbf{x}) d\mathbf{x} - \frac{1}{n} \sum_{j=0}^{n-1} f(\mathbf{x}_j) \right|^2 = \sum_{\mathbf{k} \in L^\perp \setminus \{\mathbf{0}\}} \gamma_\alpha(\mathbf{k}), \quad (58)$$

368 where  $L^\perp := \{\mathbf{k} | \mathbf{k}^\top \mathbf{z} \equiv 0 \pmod{n}, \mathbf{k} \in \mathbb{Z}^d\}$  denotes the dual lattice.

369

□

370 **Lemma 2.** Given a prime  $n$ , construct a rank-1 lattice  $\mathcal{P} = [\mathbf{x}_1, \dots, \mathbf{x}_n]$  by the generating vector  
371  $\mathbf{z} = [z_1, \dots, z_d]$ , then we have that

$$e^2(\mathcal{H}_k; \mathcal{P}) = -1 + \frac{1}{n} \sum_{j=0}^{n-1} \prod_{i=1}^d \left( \sum_{k_i \in \{1, \dots, n\}} \chi(k_i) \exp\left(2\pi i \frac{k_i j z_i}{n}\right) \right), \quad (59)$$

372 where function  $\chi(\cdot)$  on domain  $\{1, \dots, n\}$  is given as Eq.(60)

$$\chi(k_i) = \begin{cases} 1 + \frac{2}{n^\alpha} \zeta(\alpha, 1) & \text{if } k_i = n \\ \frac{1}{n^\alpha} \left( \zeta\left(\alpha, \frac{k_i}{n}\right) + \zeta\left(\alpha, \frac{n-k_i}{n}\right) \right) & \text{otherwise} \end{cases}, \quad (60)$$

373 where  $\zeta(\cdot, \cdot)$  denotes the Hurwitz zeta function.

374 *Proof.* From Lemma 1, we know that

$$e^2(\mathcal{H}_k; \mathcal{P}) = \sum_{\mathbf{k} \in \mathbb{Z}^d \setminus \{\mathbf{0}\}} \gamma_\alpha(\mathbf{k}) \left( \frac{1}{n} \sum_{j=0}^{n-1} \exp\left(2\pi i \frac{\mathbf{k}^\top \mathbf{x}_j}{n}\right) \right) \quad (61)$$

$$= -1 + \frac{1}{n} \sum_{j=0}^{n-1} \sum_{\mathbf{k} \in \mathbb{Z}^d} \gamma_\alpha(\mathbf{k}) \exp\left(2\pi i \frac{\mathbf{k}^\top \mathbf{x}_j}{n}\right) \quad (62)$$

$$= -1 + \frac{1}{n} \sum_{j=0}^{n-1} \prod_{i=1}^d \left( \sum_{k_i \in \mathbb{Z}} \gamma_\alpha(k_i) \exp\left(2\pi i \frac{k_i j z_i}{n}\right) \right) \quad (63)$$

$$= -1 + \frac{1}{n} \sum_{j=0}^{n-1} \prod_{i=1}^d \left( \sum_{k_i \in \{1, \dots, n\}} \left( \sum_{q_i \equiv k_i \pmod{n}} \gamma_\alpha(q_i) \right) \exp\left(2\pi i \frac{k_i j z_i}{n}\right) \right) \quad (64)$$

375 Now, we check the term  $\sum_{k_i \in \{1, \dots, n\}} \left( \sum_{q_i \equiv k_i \pmod{n}} \gamma_\alpha(q_i) \right)$ . From the definition of the function  
376  $\gamma_\alpha(\cdot)$ , for  $\forall k_i \in \{1, \dots, n\}$ , we have that

$$\chi(k_i) = \sum_{q_i \equiv k_i \pmod{n}} \gamma_\alpha(q_i) = \begin{cases} 1 + 2 \sum_{m=1}^{\infty} \frac{1}{(mn)^\alpha} & \text{if } k_i = n \\ \sum_{m=0}^{\infty} \frac{1}{(k_i + mn)^\alpha} + \sum_{m=0}^{\infty} \frac{1}{(n - k_i + mn)^\alpha} & \text{otherwise} \end{cases} \quad (65)$$

377 Note that series  $\sum_{m=1}^{\infty} \frac{1}{(mn)^\alpha}$ ,  $\sum_{m=0}^{\infty} \frac{1}{(k_i + mn)^\alpha}$  and  $\sum_{m=0}^{\infty} \frac{1}{(n - k_i + mn)^\alpha}$  can be rewritten as

$$\sum_{m=1}^{\infty} \frac{1}{(mn)^\alpha} = \frac{1}{n^\alpha} \sum_{m=1}^{\infty} \frac{1}{m^\alpha} = \frac{1}{n^\alpha} \zeta(\alpha, 1) \quad (66)$$

$$\sum_{m=0}^{\infty} \frac{1}{(k_i + mn)^\alpha} = \frac{1}{n^\alpha} \sum_{m=0}^{\infty} \frac{1}{\left(\frac{k_i}{n} + m\right)^\alpha} = \frac{1}{n^\alpha} \zeta\left(\alpha, \frac{k_i}{n}\right) \quad (67)$$

$$\sum_{m=0}^{\infty} \frac{1}{(n - k_i + mn)^\alpha} = \frac{1}{n^\alpha} \sum_{m=0}^{\infty} \frac{1}{\left(\frac{n - k_i}{n} + m\right)^\alpha} = \frac{1}{n^\alpha} \zeta\left(\alpha, \frac{n - k_i}{n}\right) \quad (68)$$

378 where  $\zeta(\cdot, \cdot)$  denotes the Hurwitz zeta function.

379 Plug them into Eq.(65), we know that

$$\chi(k_i) = \sum_{q_i \equiv k_i \pmod{n}} \gamma_\alpha(q_i) = \begin{cases} 1 + \frac{2}{n^\alpha} \zeta(\alpha, 1) & \text{if } k_i = n \\ \frac{1}{n^\alpha} \left( \zeta\left(\alpha, \frac{k_i}{n}\right) + \zeta\left(\alpha, \frac{n - k_i}{n}\right) \right) & \text{otherwise} \end{cases} \quad (69)$$

380 Plug Eq.(69) into Eq.(64), we have that

$$e^2(\mathcal{H}_k; \mathcal{P}) = -1 + \frac{1}{n} \sum_{j=0}^{n-1} \prod_{i=1}^d \left( \sum_{k_i \in \{1, \dots, n\}} \chi(k_i) \exp\left(2\pi i \frac{k_i j z_i}{n}\right) \right) \quad (70)$$

381

□

382 **Lemma 3.** Let  $n$  be a prime number. Let  $\gamma = [\gamma_1, \dots, \gamma_n]^\top$  be a vector with  $\gamma_k = \chi(k)$  for  
383  $k \in \{1, \dots, n\}$ , where  $\chi(\cdot)$  is defined in Lemma 2. The square worst-case integral approximation  
384 error of rank-1 lattice  $\mathcal{P}$  constructed by generating vector  $\mathbf{z} = [z_1, \dots, z_d]$  can be rewritten in a  
385 matrix form as Eq.(71)

$$e^2(\mathcal{H}_k; \mathcal{P}) = \frac{1}{n} \mathbf{1}^\top \left( \mathbf{h}^0 \odot \dots \odot \mathbf{h}^{d-1} - \mathbf{1} \right) \quad (71)$$

386 where  $\odot$  denotes the element-wise product, symbol  $\mathbf{1}$  denotes the vector with elements all ones, and  
387  $\mathbf{h}^i = \mathbf{F}^i \gamma$  with  $\mathbf{F}$  as the discrete Fourier matrix, i.e.,  $\mathbf{F}_{jk} = \exp(2\pi i \frac{jk}{n})$ , and  $\mathbf{F}^i$  denotes the matrix  
388 after permutation of the rows of  $\mathbf{F}$  such that the  $j^{\text{th}}$  row of  $\mathbf{F}^i$  equals to the  $\tilde{j}^{\text{th}}$  row of  $\mathbf{F}$ , where  
389  $\tilde{j} = j z_{i+1} \bmod n$ .

390 *Proof.* Define  $\mathbf{h}^i$  as Eq.(72)

$$\mathbf{h}^i = \mathbf{F}^i \gamma \quad (72)$$

391 where  $\mathbf{F}$  as the discrete Fourier matrix, i.e.,  $\mathbf{F}_{jk} = \exp(2\pi i \frac{jk}{n})$ , and  $\mathbf{F}^i$  denotes the matrix after  
392 permutation of the rows of  $\mathbf{F}$  such that the  $j^{\text{th}}$  row of  $\mathbf{F}^i$  equals to the  $\tilde{j}^{\text{th}}$  row of  $\mathbf{F}$ , where  
393  $\tilde{j} = j z_{i+1} \bmod n$ , and  $g$  denotes the primitive root modulo  $n$ .

394 From Lemma 2, we know that

$$e^2(\mathcal{H}_k; \mathcal{P}) = -1 + \frac{1}{n} \sum_{j=0}^{n-1} \prod_{i=1}^d \left( \sum_{k_i \in \{1, \dots, n\}} \chi(k_i) \exp\left(2\pi i \frac{k_i j z_i}{n}\right) \right) \quad (73)$$

395 Note that  $\gamma = [\gamma_1, \dots, \gamma_n]^\top$  is a vector with  $\gamma_k = \chi(k)$  for  $k \in \{1, \dots, n\}$ , it follows that

$$e^2(\mathcal{H}_k; \mathcal{P}) = -1 + \frac{1}{n} \mathbf{1}^\top \left( \mathbf{F}^0 \gamma \odot \dots \odot \mathbf{F}^{d-1} \gamma \right) \quad (74)$$

$$= -1 + \frac{1}{n} \mathbf{1}^\top \left( \mathbf{h}^0 \odot \dots \odot \mathbf{h}^{d-1} \right) \quad (75)$$

$$= \frac{1}{n} \mathbf{1}^\top \left( \mathbf{h}^0 \odot \dots \odot \mathbf{h}^{d-1} - \mathbf{1} \right) \quad (76)$$

396 □

397 **Lemma 4.** Let  $n$  be a prime number such that  $(2d-1)|(n-1)$ . Let  $\gamma = [\gamma_1, \dots, \gamma_n]^\top$  be a vector  
398 with  $\gamma_k = \chi(k)$  for  $k \in \{1, \dots, n\}$ , where  $\chi(\cdot)$  is defined in Lemma 2. Given a rank-1 lattice  $\mathcal{P}$   
399 constructed by generating vector in Eq.(31), then we have Eq.(77)

$$\begin{aligned} \mathbf{1}^\top (\mathbf{h}^0 \odot \dots \odot \mathbf{h}^{d-1} - \mathbf{1}) &= \mathbf{1}^\top (\mathbf{h}^d \odot \dots \odot \mathbf{h}^{2d-2} - \mathbf{1}) + \langle \mathbf{h}^d \odot \dots \odot \mathbf{h}^{2d-2} - \mathbf{1}, \mathbf{h}^0 - \mathbf{1} \rangle \\ &\quad + \mathbf{1}^\top (\mathbf{h}^0 - \mathbf{1}) \end{aligned} \quad (77)$$

400 where  $\odot$  denotes the element-wise product, symbol  $\mathbf{1}$  denotes the vector with elements all ones, and  
401  $\mathbf{h}^i = \mathbf{F}^i \gamma$  with  $\mathbf{F}$  as the discrete Fourier matrix, i.e.,  $\mathbf{F}_{jk} = \exp(2\pi i \frac{jk}{n})$ , and  $\mathbf{F}^i$  denotes the matrix  
402 after permutation of the rows of  $\mathbf{F}$  such that the  $j^{\text{th}}$  row of  $\mathbf{F}^i$  equals to the  $\tilde{j}^{\text{th}}$  row of  $\mathbf{F}$ , where  
403  $\tilde{j} = j g^{\frac{i(n-1)}{2d-1}} \bmod n$ , and  $g$  denotes the primitive root modulo  $n$ .

404 *Proof.* Note that  $\mathbf{h}^i = \mathbf{F}^i \gamma$  is a permutation of  $\mathbf{h}^0$ . From the definition of permutation  $\mathbf{F}^i$ , we know  
405 that the  $j^{\text{th}}$  row of  $\mathbf{F}^i$  equals to the  $\tilde{j}^{\text{th}}$  row of  $\mathbf{F}$  with  $\tilde{j} = j g^{\frac{i(n-1)}{2d-1}} \bmod n$ . Note that  $(2d-1)|(n-1)$   
406 and  $n$  is a prime number, we know  $\{1, g^{\frac{1(n-1)}{2d-1}}, \dots, g^{\frac{(2d-2)(n-1)}{2d-1}}\}$  modulo  $n$  forms a subgroup of  
407  $\{1, \dots, n-1\}$  modulo  $n$ . Thus, we know  $\{\mathbf{h}^0, \mathbf{h}^1, \dots, \mathbf{h}^{2d-2}\}$  forms a group, and  $\mathbf{h}^0 = \mathbf{h}^{2d-1}$ .  
408 Furthermore, we know that  $\mathbf{h}^k$  is a permutation of  $\mathbf{h}^i$  such that  $j^{\text{th}}$  row of  $\mathbf{F}^k$  equals to the  $\bar{j}^{\text{th}}$  row  
409 of  $\mathbf{F}^i$  with  $\bar{j} = j g^{\frac{(k-i)(n-1)}{2d-1}} \bmod n$ . Thus, we know that

$$\mathbf{1}^\top (\mathbf{h}^0 \odot \dots \odot \mathbf{h}^{d-1}) = \mathbf{1}^\top (\mathbf{h}^d \odot \dots \odot \mathbf{h}^{2d-1}) \quad (78)$$

410 Note that  $\mathbf{h}^0 = \mathbf{h}^{2d-1}$ . It follows that

$$\mathbf{1}^\top (\mathbf{h}^0 \odot \dots \odot \mathbf{h}^{d-1} - \mathbf{1}) = \mathbf{1}^\top (\mathbf{h}^d \odot \dots \odot \mathbf{h}^{2d-1} - \mathbf{1}) \quad (79)$$

$$= \mathbf{1}^\top (\mathbf{h}^d \odot \dots \odot \mathbf{h}^{2d-2} \odot \mathbf{h}^0 - \mathbf{1}) \quad (80)$$

411 In addition, we have that

$$\langle \mathbf{h}^d \odot \dots \odot \mathbf{h}^{2d-2} - \mathbf{1}, \mathbf{h}^0 - \mathbf{1} \rangle \quad (81)$$

$$= \langle \mathbf{h}^d \odot \dots \odot \mathbf{h}^{2d-2}, \mathbf{h}^0 \rangle - \mathbf{1}^\top (\mathbf{h}^d \odot \dots \odot \mathbf{h}^{2d-2}) - \mathbf{1}^\top \mathbf{h}^0 + \mathbf{1}^\top \mathbf{1} \quad (82)$$

$$= \mathbf{1}^\top (\mathbf{h}^d \odot \dots \odot \mathbf{h}^{2d-2} \odot \mathbf{h}^0) - \mathbf{1}^\top (\mathbf{h}^d \odot \dots \odot \mathbf{h}^{2d-2}) - \mathbf{1}^\top \mathbf{h}^0 + \mathbf{1}^\top \mathbf{1} \quad (83)$$

$$= \mathbf{1}^\top (\mathbf{h}^d \odot \dots \odot \mathbf{h}^{2d-2} \odot \mathbf{h}^0) - \mathbf{1}^\top \mathbf{1} - \mathbf{1}^\top (\mathbf{h}^d \odot \dots \odot \mathbf{h}^{2d-2}) + \mathbf{1}^\top \mathbf{1} - \mathbf{1}^\top \mathbf{h}^0 + \mathbf{1}^\top \mathbf{1} \quad (84)$$

$$= \mathbf{1}^\top (\mathbf{h}^d \odot \dots \odot \mathbf{h}^{2d-2} \odot \mathbf{h}^0 - \mathbf{1}) - \mathbf{1}^\top (\mathbf{h}^d \odot \dots \odot \mathbf{h}^{2d-2} - \mathbf{1}) - \mathbf{1}^\top (\mathbf{h}^0 - \mathbf{1}) \quad (85)$$

412 It follows that

$$\begin{aligned} \mathbf{1}^\top (\mathbf{h}^d \odot \dots \odot \mathbf{h}^{2d-2} \odot \mathbf{h}^0 - \mathbf{1}) &= \langle \mathbf{h}^d \odot \dots \odot \mathbf{h}^{2d-2} - \mathbf{1}, \mathbf{h}^0 - \mathbf{1} \rangle + \mathbf{1}^\top (\mathbf{h}^d \odot \dots \odot \mathbf{h}^{2d-2} - \mathbf{1}) \\ &\quad + \mathbf{1}^\top (\mathbf{h}^0 - \mathbf{1}) \end{aligned} \quad (86)$$

413 Plug Eq.(86) into Eq.(80), we know that

$$\begin{aligned} \mathbf{1}^\top (\mathbf{h}^0 \odot \dots \odot \mathbf{h}^{d-1} - \mathbf{1}) &= \langle \mathbf{h}^d \odot \dots \odot \mathbf{h}^{2d-2} - \mathbf{1}, \mathbf{h}^0 - \mathbf{1} \rangle + \mathbf{1}^\top (\mathbf{h}^d \odot \dots \odot \mathbf{h}^{2d-2} - \mathbf{1}) \\ &\quad + \mathbf{1}^\top (\mathbf{h}^0 - \mathbf{1}) \end{aligned} \quad (87)$$

414

□

415 **Lemma 5.** Let  $n$  be a prime number such that  $(2d-1)|(n-1)$ . Let  $\boldsymbol{\gamma} = [\gamma_1, \dots, \gamma_n]^\top$  be a vector  
416 with  $\gamma_k = \chi(k)$  for  $k \in \{1, \dots, n\}$ , where  $\chi(\cdot)$  is defined in Lemma 2. Given a rank-1 lattice  $\mathcal{P}$   
417 constructed by generating vector in Eq.(31), then we have Eq.(88)

$$\begin{aligned} \mathbf{1}^\top (\mathbf{h}^0 \odot \dots \odot \mathbf{h}^{2d-2} - \mathbf{1}) &= \mathbf{1}^\top (\mathbf{h}^0 \odot \dots \odot \mathbf{h}^{d-1} - \mathbf{1}) + \mathbf{1}^\top (\mathbf{h}^d \odot \dots \odot \mathbf{h}^{2d-2} - \mathbf{1}) \\ &\quad + \langle \mathbf{h}^0 \odot \dots \odot \mathbf{h}^{d-1} - \mathbf{1}, \mathbf{h}^d \odot \dots \odot \mathbf{h}^{2d-2} - \mathbf{1} \rangle \end{aligned} \quad (88)$$

418 where  $\odot$  denotes the element-wise product, symbol  $\mathbf{1}$  denotes the vector with elements all ones, and  
419  $\mathbf{h}^i = \mathbf{F}^i \boldsymbol{\gamma}$  with  $\mathbf{F}$  as the discrete Fourier matrix, i.e.,  $\mathbf{F}_{jk} = \exp(2\pi i \frac{jk}{n})$ , and  $\mathbf{F}^i$  denotes the matrix  
420 after permutation of the rows of  $\mathbf{F}$  such that the  $j^{\text{th}}$  row of  $\mathbf{F}^i$  equals to the  $\tilde{j}^{\text{th}}$  row of  $\mathbf{F}$ , where  
421  $\tilde{j} = jg \frac{i(n-1)}{2d-1} \bmod n$ , and  $g$  denotes the primitive root modulo  $n$ .

422 *Proof.* Similar to the proof of Lemma 4, we have that

$$\langle \mathbf{h}^0 \odot \dots \odot \mathbf{h}^{d-1} - \mathbf{1}, \mathbf{h}^d \odot \dots \odot \mathbf{h}^{2d-2} - \mathbf{1} \rangle \quad (89)$$

$$= \langle \mathbf{h}^0 \odot \dots \odot \mathbf{h}^{d-1}, \mathbf{h}^d \odot \dots \odot \mathbf{h}^{2d-2} \rangle - \mathbf{1}^\top (\mathbf{h}^0 \odot \dots \odot \mathbf{h}^{d-1}) - \mathbf{1}^\top (\mathbf{h}^d \odot \dots \odot \mathbf{h}^{2d-2}) + \mathbf{1}^\top \mathbf{1} \quad (90)$$

$$= \mathbf{1}^\top (\mathbf{h}^0 \odot \dots \odot \mathbf{h}^{2d-2}) - \mathbf{1}^\top (\mathbf{h}^0 \odot \dots \odot \mathbf{h}^{d-1}) - \mathbf{1}^\top (\mathbf{h}^d \odot \dots \odot \mathbf{h}^{2d-2}) + \mathbf{1}^\top \mathbf{1} \quad (91)$$

$$= \mathbf{1}^\top (\mathbf{h}^0 \odot \dots \odot \mathbf{h}^{2d-2}) - \mathbf{1}^\top \mathbf{1} - \mathbf{1}^\top (\mathbf{h}^0 \odot \dots \odot \mathbf{h}^{d-1}) + \mathbf{1}^\top \mathbf{1} - \mathbf{1}^\top (\mathbf{h}^d \odot \dots \odot \mathbf{h}^{2d-2}) + \mathbf{1}^\top \mathbf{1} \quad (92)$$

$$= \mathbf{1}^\top (\mathbf{h}^0 \odot \dots \odot \mathbf{h}^{2d-2} - \mathbf{1}) - \mathbf{1}^\top (\mathbf{h}^0 \odot \dots \odot \mathbf{h}^{d-1} - \mathbf{1}) - \mathbf{1}^\top (\mathbf{h}^d \odot \dots \odot \mathbf{h}^{2d-2} - \mathbf{1}) \quad (93)$$

423 It follows that

$$\begin{aligned} \mathbf{1}^\top (\mathbf{h}^0 \odot \dots \odot \mathbf{h}^{2d-2} - \mathbf{1}) &= \mathbf{1}^\top (\mathbf{h}^0 \odot \dots \odot \mathbf{h}^{d-1} - \mathbf{1}) + \mathbf{1}^\top (\mathbf{h}^d \odot \dots \odot \mathbf{h}^{2d-2} - \mathbf{1}) \\ &\quad + \langle \mathbf{h}^0 \odot \dots \odot \mathbf{h}^{d-1} - \mathbf{1}, \mathbf{h}^d \odot \dots \odot \mathbf{h}^{2d-2} - \mathbf{1} \rangle \end{aligned} \quad (94)$$

424

□



425 **Lemma 6.** Let  $n$  be a prime number such that  $(2d-1)|(n-1)$ . Let  $\gamma = [\gamma_1, \dots, \gamma_n]^\top$  be a vector  
426 with  $\gamma_k = \chi(k)$  for  $k \in \{1, \dots, n\}$ , where  $\chi(\cdot)$  is defined in Lemma 2. Given a rank-1 lattice  $\mathcal{P}$   
427 constructed by generating vector in Eq.(31), then we have Eq.(95)

$$\begin{aligned} \mathbf{1}^\top(\mathbf{h}^0 \odot \dots \odot \mathbf{h}^{2d-2} - \mathbf{1}) &= \mathbf{1}^\top((\mathbf{h}^1 \odot \dots \odot \mathbf{h}^{d-1} - \mathbf{1}) \odot \mathbf{h}^0 \odot (\mathbf{h}^{-(d-1)} \odot \dots \odot \mathbf{h}^{-1} - \mathbf{1})) \\ &\quad + 2\mathbf{1}^\top(\mathbf{h}^0 \odot \dots \odot \mathbf{h}^{d-1} - \mathbf{1}) - \mathbf{1}^\top(\mathbf{h}^0 - \mathbf{1}) \end{aligned} \quad (95)$$

428 where  $\odot$  denotes the element-wise product, symbol  $\mathbf{1}$  denotes the vector with elements all ones, and  
429  $\mathbf{h}^i = \mathbf{F}^i \gamma$  with  $\mathbf{F}$  as the discrete Fourier matrix, i.e.,  $\mathbf{F}_{jk} = \exp(2\pi i \frac{jk}{n})$ , and  $\mathbf{F}^i$  denotes the matrix  
430 after permutation of the rows of  $\mathbf{F}$  such that the  $j^{\text{th}}$  row of  $\mathbf{F}^i$  equals to the  $\tilde{j}^{\text{th}}$  row of  $\mathbf{F}$ , where  
431  $\tilde{j} = jg \frac{i(n-1)}{2d-1} \bmod n$ , and  $g$  denotes the primitive root modulo  $n$ .

432 *Proof.* Plug Eq.(77) in Lemma 4 into Eq.(88) in Lemma 5, we know that

$$\begin{aligned} \mathbf{1}^\top(\mathbf{h}^0 \odot \dots \odot \mathbf{h}^{2d-2} - \mathbf{1}) &= 2\mathbf{1}^\top(\mathbf{h}^0 \odot \dots \odot \mathbf{h}^{d-1} - \mathbf{1}) - \mathbf{1}^\top(\mathbf{h}^0 - \mathbf{1}) - \langle \mathbf{h}^d \odot \dots \odot \mathbf{h}^{2d-2} - \mathbf{1}, \mathbf{h}^0 - \mathbf{1} \rangle \\ &\quad + \langle \mathbf{h}^0 \odot \dots \odot \mathbf{h}^{d-1} - \mathbf{1}, \mathbf{h}^d \odot \dots \odot \mathbf{h}^{2d-2} - \mathbf{1} \rangle \end{aligned} \quad (96)$$

433 Now we check the last two terms in Eq.(96). Note that

$$\langle \mathbf{h}^0 \odot \dots \odot \mathbf{h}^{d-1} - \mathbf{1}, \mathbf{h}^d \odot \dots \odot \mathbf{h}^{2d-2} - \mathbf{1} \rangle - \langle \mathbf{h}^d \odot \dots \odot \mathbf{h}^{2d-2} - \mathbf{1}, \mathbf{h}^0 - \mathbf{1} \rangle \quad (97)$$

$$= \langle \mathbf{h}^0 \odot \dots \odot \mathbf{h}^{d-1} - \mathbf{1} - (\mathbf{h}^0 - \mathbf{1}), \mathbf{h}^d \odot \dots \odot \mathbf{h}^{2d-2} - \mathbf{1} \rangle \quad (98)$$

$$= \langle \mathbf{h}^0 \odot \dots \odot \mathbf{h}^{d-1} - \mathbf{h}^0, \mathbf{h}^d \odot \dots \odot \mathbf{h}^{2d-2} - \mathbf{1} \rangle \quad (99)$$

$$= \langle \mathbf{h}^0 \odot (\mathbf{h}^1 \odot \dots \odot \mathbf{h}^{d-1} - \mathbf{1}), \mathbf{h}^d \odot \dots \odot \mathbf{h}^{2d-2} - \mathbf{1} \rangle \quad (100)$$

$$= \mathbf{1}^\top((\mathbf{h}^1 \odot \dots \odot \mathbf{h}^{d-1} - \mathbf{1}) \odot \mathbf{h}^0 \odot (\mathbf{h}^d \odot \dots \odot \mathbf{h}^{2d-2} - \mathbf{1})) \quad (101)$$

434 It follows that

$$\begin{aligned} \mathbf{1}^\top(\mathbf{h}^0 \odot \dots \odot \mathbf{h}^{2d-2} - \mathbf{1}) &= 2\mathbf{1}^\top(\mathbf{h}^0 \odot \dots \odot \mathbf{h}^{d-1} - \mathbf{1}) - \mathbf{1}^\top(\mathbf{h}^0 - \mathbf{1}) \\ &\quad + \mathbf{1}^\top((\mathbf{h}^1 \odot \dots \odot \mathbf{h}^{d-1} - \mathbf{1}) \odot \mathbf{h}^0 \odot (\mathbf{h}^d \odot \dots \odot \mathbf{h}^{2d-2} - \mathbf{1})) \end{aligned} \quad (102)$$

435 Because  $\{\mathbf{h}^0, \mathbf{h}^1, \dots, \mathbf{h}^{2d-2}\}$  forms a group, and  $\mathbf{h}^0 = \mathbf{h}^{2d-1}$  with a modulo period  $2d-1$ , we  
436 know that

$$\mathbf{h}^d \odot \dots \odot \mathbf{h}^{2d-2} = \mathbf{h}^{-(d-1)} \odot \dots \odot \mathbf{h}^{-1} \quad (103)$$

437 Plug Eq.(103) into Eq.(102), we have that

$$\begin{aligned} \mathbf{1}^\top(\mathbf{h}^0 \odot \dots \odot \mathbf{h}^{2d-2} - \mathbf{1}) &= 2\mathbf{1}^\top(\mathbf{h}^0 \odot \dots \odot \mathbf{h}^{d-1} - \mathbf{1}) - \mathbf{1}^\top(\mathbf{h}^0 - \mathbf{1}) \\ &\quad + \mathbf{1}^\top((\mathbf{h}^1 \odot \dots \odot \mathbf{h}^{d-1} - \mathbf{1}) \odot \mathbf{h}^0 \odot (\mathbf{h}^{-d-1} \odot \dots \odot \mathbf{h}^{-1} - \mathbf{1})) \end{aligned} \quad (104)$$

438 □

439 Now, we are ready to prove our main Theorem 1.

440 *Proof.* From Lemma 3, we know that

$$e^2(\mathcal{H}_k; \mathcal{P}) = \frac{1}{n} \mathbf{1}^\top(\mathbf{h}^0 \odot \dots \odot \mathbf{h}^{d-1} - \mathbf{1}) \quad (105)$$

441 From Lemma 6, we know that

$$\begin{aligned} &\mathbf{1}^\top(\mathbf{h}^0 \odot \dots \odot \mathbf{h}^{d-1} - \mathbf{1}) \\ &= \frac{1}{2} \mathbf{1}^\top(\mathbf{h}^0 \odot \dots \odot \mathbf{h}^{2d-2} - \mathbf{1} - (\mathbf{h}^1 \odot \dots \odot \mathbf{h}^{d-1} - \mathbf{1}) \odot \mathbf{h}^0 \odot (\mathbf{h}^{-1} \odot \dots \odot \mathbf{h}^{-(d-1)} - \mathbf{1})) \\ &\quad + \frac{1}{2} \mathbf{1}^\top(\mathbf{h}^0 - \mathbf{1}) \end{aligned} \quad (106)$$

442 Plug Eq.(106) into Eq.(105), we have that

$$\begin{aligned}
& e^2(\mathcal{H}_k; \mathcal{P}) \\
&= \frac{1}{2n} \mathbf{1}^\top (\mathbf{h}^0 \odot \dots \odot \mathbf{h}^{2d-2} - \mathbf{1} - (\mathbf{h}^1 \odot \dots \odot \mathbf{h}^{d-1} - \mathbf{1}) \odot \mathbf{h}^0 \odot (\mathbf{h}^{-1} \odot \dots \odot \mathbf{h}^{-(d-1)} - \mathbf{1})) \\
&+ \frac{1}{2n} \mathbf{1}^\top (\mathbf{h}^0 - \mathbf{1})
\end{aligned} \tag{107}$$

443 Note that  $\mathbf{h}^0 = \mathbf{F}\boldsymbol{\gamma}$  and  $\mathbf{F}$  denotes the discrete Fourier matrix, we have that

$$\mathbf{1}^\top (\mathbf{h}^0 - \mathbf{1}) = \mathbf{1}^\top \mathbf{F}\boldsymbol{\gamma} - n \tag{108}$$

$$= \mathbf{b}^\top \boldsymbol{\gamma} - n \tag{109}$$

444 where  $\mathbf{b} = [0, 0, \dots, 0, n]^\top$ .

445 Note that the  $n^{\text{th}}$  element in  $\boldsymbol{\gamma}$  is  $\gamma_n = 1 + \frac{2}{n^\alpha} \zeta(\alpha, 1)$ , where  $\zeta(\cdot, \cdot)$  denotes the Hurwitz zeta function.

446 It follows that

$$\mathbf{1}^\top (\mathbf{h}^0 - \mathbf{1}) = \mathbf{b}^\top \boldsymbol{\gamma} - n = n + n \frac{2}{n^\alpha} \zeta(\alpha, 1) - n = n \frac{2}{n^\alpha} \zeta(\alpha, 1) \tag{110}$$

447 Plug Eq.(110) into Eq.(107), we achieve the result in Theorem 1

$$\begin{aligned}
& e^2(\mathcal{H}_k; \mathcal{P}) \\
&= \frac{1}{2n} \mathbf{1}^\top (\mathbf{h}^0 \odot \dots \odot \mathbf{h}^{2d-2} - \mathbf{1} - (\mathbf{h}^1 \odot \dots \odot \mathbf{h}^{d-1} - \mathbf{1}) \odot \mathbf{h}^0 \odot (\mathbf{h}^{-1} \odot \dots \odot \mathbf{h}^{-(d-1)} - \mathbf{1})) \\
&+ \frac{1}{n^\alpha} \zeta(\alpha, 1)
\end{aligned} \tag{111}$$

448

□

## 449 B Benchmark Test Functions

450 The benchmark test functions employed in section 4.1 are listed in Table 1, which contains multi-mode  
451 functions and non-smooth functions that are challenging for optimization.

Table 1: Test functions

name	function
Rosenbrock	$\sum_{i=1}^{d-1} \left( 100(x_{i+1} - x_i^2)^2 + (1 - x_i)^2 \right)$
Nesterov	$\frac{1}{4}  x_1 - 1  + \sum_{i=1}^{d-1}  x_{i+1} - 2 x_i  + 1 $
Rastrigin	$10d + \sum_{i=1}^d (x_i^2 - 10 \cos(2\pi x_i))$

452 **C Training Time and Fast Coordinate Search Time**

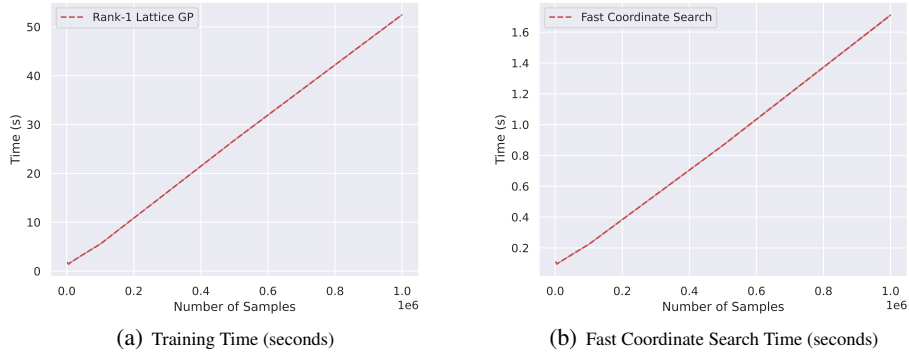


Figure 4: Training Time and Fast Coordinate Search Time (seconds) v.s. the number of samples

453 We provide the training time of our rank- 1 lattice GP and the time of our fast coordinate  
 454 search for targeted sampling in Figure 4(a) and Figure 4(b), respectively. The dimension of  
 455 the rank-1 lattice data is set to  $d = 50$ . The number of samples  $n$  is set to the parameter in  
 456  $\{1783, 5347, 10099, 51283, 100189, 501139, 1000099\}$ . The number of samples  $n$  is a prime num-  
 457 ber such that  $(2d - 1)|(n - 1)$  to achieve our closed-form rank-1 lattice construction. The number of  
 458 epochs of training is set to 2000. The number of iterations of fast coordinate search is set to  $T = 50$ .  
 459 All the experiments are performed in 50 runs on a single NVIDIA A40 card.

460 We report the mean value  $\pm$  std in Figure 4. The standard deviation of the time is small. From  
 461 Figure 4(a), we can see that it takes around 50 seconds for our rank-1 GP training with one million  
 462 lattice data. Moreover, our fast coordinate search for targeted sampling takes around 1.5 seconds to  
 463 optimize rank-1 lattice GP posterior prediction conditioned on one million lattice data.

464 **D Additional Experiments of Black-box Prompt Fine-tuning**

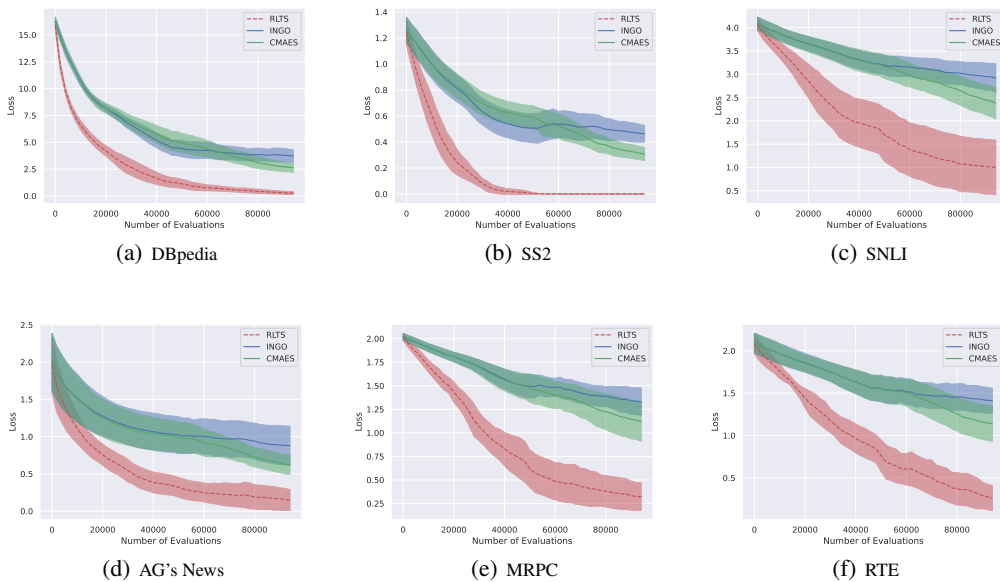


Figure 5: Hinge loss v.s. the number of queries on different black-box fine-tuning models.

465 We provide additional experimental results of black-box prompt fine-tuning for large language models.  
466 We employ the deep model in Sun et al. [2022a] as the backbone. It has 24 layers. For each layer,  
467 we set the dimension of the continuous prompt to 500. Thus, the total dimension is  $24 \times 500$ . We  
468 employ the hinge loss of training data as the black-box objective.

469 In all the experiments, we keep the number of batch samples and the initialization the same for RLTS,  
470 INGO and CMAES. We set the number of batch samples to 2000. Our RLTS employs 1999 rank-1  
471 lattice QMC Gaussian samples and one sample from targeted sampling. INGO employs 1999 rank-1  
472 lattice QMC Gaussian samples and one Gaussian sample. CMAES employs 2000 Gaussian samples.  
473 We initialize the  $\mu = \mathbf{0}$  for all the methods. For INGO and RLTS, we set the step-size parameter  
474  $\beta = 0.2$  in all experiments. For RLTS, we set the parameter  $\eta = 1$  in all experiments. All the  
475 experiments are performed in five independent runs with seeds in  $\{1, 2, 3, 4, 5\}$ .

476 The experimental results of mean objective  $\pm$  std v.s. the number of queries are shown in Figure 5.  
477 From Figure 5, we can observe that our RLTS decreases the objective significantly faster than INGO  
478 and CMAES on all six fine-tuning tasks, which shows the superior query efficiency of our RLTS.